ISSN 0280-5316
ISRN LUTFD2/TFRT--5902--SE

Optimal Control Algorithms for Klystron Efficiency in ESS

Josefin Berner
Aminda Ingulfson

Lund University
Department of Automatic Control
June 2012

Lund University
Department of Automatic Control
Box 118
SE-221 00 Lund Sweden

Document name
MASTER THESIS

Date of issue
June 2012

Document Number
ISRN LUTFD2/TFRT--5902--SE

Author(s)
Josefin Berner
Aminda Ingulfson

Supervisor
Anders J Johansson, Dept. of Electrical and Information Technology, Lund University, Sweden
Rolf Johansson, Dept. of Automatic Control, Lund University, Sweden (examiner)

Sponsoring organization

Title and subtitle
Optimal Control Algorithms for Klystron Efficiency in ESS (Optimal reglering för klystroneffektivitet i ESS)

Abstract
European Spallation Source (ESS) is a linear particle accelerator planned to be built in Lund, Sweden. There is a need to control the electric field in the cavities in the particle accelerator, according to given specifications of the field. The aim of this thesis is to compare a traditional PI controller to an MPC controller, to see if there is any difference in the performance that can be achieved. One important aspect of the performance analysis is to see whether the klystron efficiency could be increased with either of the controllers. Since ESS is planned to open 2019 and to be fully operational 2025, the evaluation will be based on simulation results in Matlab/Simulink. To be able to do the comparisons a model of the entire system, a realistic model of the klystron, a PI controller and an MPC controller have been implemented.
Both the PI controller and the MPC controller give satisfying results in normal operation. The klystron efficiency could be increased with the MPC controller, and probably with the PI controller as well.

Keywords
European Spallation Source (ESS), Particle accelerator, PI controller, MPC controller, Klystron, Cavity, Matlab, Simulink

Classification system and/ or index terms (if any)

Supplementary bibliographical information

ISSN and key title
0280-5316

ISBN

Language
English

Number of pages
1-57

Recipient's notes

Security classification

Abstract

European Spallation Source (ESS) is a linear particle accelerator planned to be built in Lund, Sweden. There is a need to control the electric field in the cavities in the particle accelerator, according to given specifications of the field. The aim of this thesis is to compare a traditional PI controller to an MPC controller, to see if there is any difference in the performance that can be achieved. One important aspect of the performance analysis is to see whether the klystron efficiency could be increased with either of the controllers.

Since ESS is planned to open 2019 and to be fully operational 2025, the evaluation will be based on simulation results in Matlab/Simulink. To be able to do the comparisons a model of the entire system, a realistic model of the klystron, a PI controller and an MPC controller have been implemented.

Both the PI controller and the MPC controller give satisfying results in normal operation. The klystron efficiency could be increased with the MPC controller, and probably with the PI controller as well.

Keywords: European Spallation Source (ESS), Particle accelerator, PI controller, MPC controller, Klystron, Cavity, Matlab, Simulink.

Sammanfattning

European Spallation Source (ESS) är en linjäraccelerator som kommer att byggas i Lund, Sverige. Det finns ett behov av att reglera det elektriska fältet i kaviteterna i acceleratorn enligt givna specifikationer för fältet. Syftet med arbetet är att jämföra den vanligare PI regulatorn med en MPC regulator för att se om det är någon skillnad i prestandan. En viktig synpunkt i jämförelsen är att se om klystroneffektiviteten kan ökas med någon av regulatorerna.

Eftersom ESS är i planeringsstadiet och först kommer vara i full drift 2025 så baseras utvärderingen på resultat från simuleringar i Matlab/Simulink. För att kunna jämföra regulatorerna har en modell av hela systemet, en realistisk modell av klystronen, en PI regulator och en MPC regulator implementerats.

Både PI regulatorn och MPC regulatorn ger tillfredställande resultat vid normal drift. Klystroneffektiviteten kan förbättras med en MPC regualtor, och troligen även med en PI regulator.

Acknowledgements

This master's thesis was conducted at the Department of Automatic Control, Lund University, in collaboration with the European Spallation Source ESS AB. The work was performed in the spring of 2012.

We would like to thank our supervisors Rolf Johansson (Automatic Control) and Anders J Johansson (Electrical and Information Technology). We would also like to thank Rihua Zeng and Stephen Molloy at ESS AB for some valuable clarifications. We want to thank Anders Nilsson (Automatic Control) for helping us with all kinds of computer-related issues.

We also want to thank Cem Eliyürekli for his love of correcting other peoples reports, Babak Rajabian and Arnbjörn Einarsson for all cooperation and shared frustration, and everyone at the Department of Automatic Control for amusing and interesting conversations during the coffee-breaks.

Josefin and Aminda

Contents

1. Introduction

1.1 Aim of thesis

There is a need to control the electric field in the cavities in ESS's particle accelerator, according to given specifications of the field. The control system for this task could be designed in many different ways. The aim of this thesis is to compare a traditional PI controller to an MPC controller, to see if there is any difference in the performance that can be achieved. One important aspect of the performance is to see whether the klystron efficiency could be increased with either of the controllers.

The evaluation will be based on simulation results in Matlab/Simulink. To be able to do the comparisons a model of the entire system, with a realistic model of the klystron, a PI controller and an MPC controller, is needed.

1.2 Outline of report

The outline of this report is that the theoretical background needed to describe all the components of the system is given in Chapter 2. The implementation details are described in Chapter 3. The methodology of the tests performed is described in Chapter 4. The results will then be listed in Chapter 5 followed by discussion and conclusion in Chapters 6 and 7.

1.3 European Spallation Source (ESS)

European Spallation Source (ESS) is a research facility under development in Lund, Sweden. Seventeen European countries[1] are participating in the project, which is planned to open in 2019 and be fully operational in 2025. By accelerating protons to almost the speed of light and then colliding them with a target of tungsten, neutrons will be released from the target and led out to 22 independent experimental stations, as shown in Figure 1.1 [3, Ch.2].

In the experimental stations the neutrons are used for different material studies. Neutrons work in a similar way to X-rays, but the resulting images show different parts of the object. Neutrons give good pictures of carbon, nitrogen and oxygen that are all important to life [6]. They can also distinguish between different isotopes of hydrogen. These abilities together with the fact that neutrons do not damage sensitive samples such as living cells, makes it a great alternative for closer studies of for example proteins and DNA. It is also an important tool to make cancer treatment more efficient. With neutrons the image of the sick area will be sharper and more detailed, which makes it easier to only treat cancer cells and fewer healthy cells [3, Ch.2].

Neutrons are also important in the environmental area. Research to make rechargeable, longer-lasting, more efficient and environmentally friendly batteries and to find more efficient and environmentally friendly catalysts could for example make future cars less polluting [3, Ch.2].

Another important area of research is to develop usable alloys like titanium and high-strength aluminium. This could for example give lighter airplanes, meaning less usage of fuel which would be good for the nature [3, Ch.2]. Some other areas where neutrons can be used for research are biofuel, cosmetics, detergents, paint, nanoscience, medicine, food technology, combustion, packaging and geoscience [7].

[1] Sweden, Denmark, Norway, Latvia, Lithuania, Estonia, Iceland, Poland, Germany, France, the United Kingdom, the Netherlands, Hungary, the Czech Republic, Switzerland, Spain, and Italy.

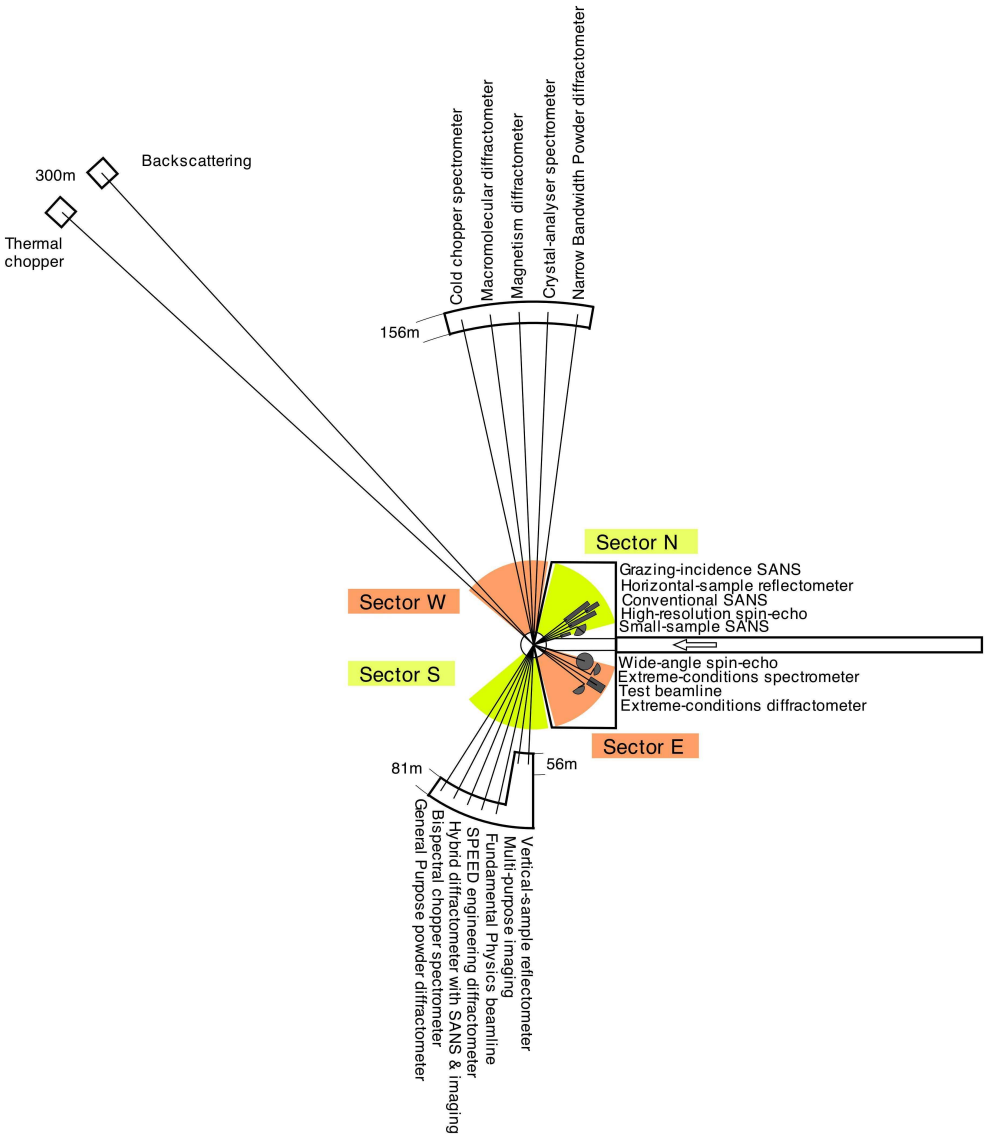

Figure 1.1 An overview of the experimental stations in ESS [3, Ch.2].

The ESS accelerator

The schematics of the particle accelerator are shown in Figure 1.2. The proton beam enters the accelerator from the proton source and then passes a number of cavities on its way to the target. The cavities have electric fields with alternating polarity, which accelerate the protons to very high energies [11, Ch.4].

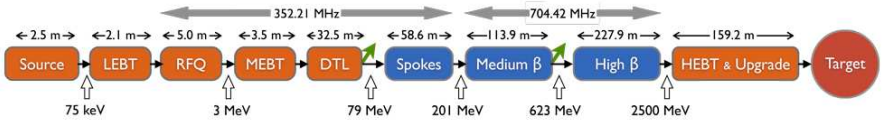

Figure 1.2 Schematic picture of the accelerator, May 2012. The blocks between the source and the target are the different kinds of cavities that will be used [5].

The accelerator can be broken down to many small subsystems that each contains a cavity, a klystron (basically an amplifier), a circulator and a Low Level Radio Frequency (LLRF) system that includes the controller [3]. A schematic diagram of this can be seen in Figure 1.3.

The basic idea is that the field of the cavity is measured and the measurements enter the controller. The controller compares the actual values with the references and calculates a new control signal in the shape of a voltage. This signal is sent to the klystron that amplifies it and passes it on to the cavity. The purpose of the circulator is to make sure that no reflected waves from the cavity enters the klystron, since that could destroy the klystron. Another good thing about the circulator is that it makes sure that the klystron sees a constant load, as to not be affected by the so called pulling effect. The functionality of the different parts will be described in more detail in Chapter 2.

The easiest way to control the system is if the klystron is assumed to be linear. However, the klystron can only be viewed as linear in an area where the efficiency of it is low. To be able to use the klystron more efficiently, the operation of it must move to its non-linear area. Every improvement of the efficiency of the klystron will reduce the amount of waste energy in ESS and hence save both energy and money.

As can be seen in Figure 1.2 there are a number of different cavity types. The focus of this thesis will be on the high β elliptical cavities, since they outnumber the others and will be contributing the most to the energy consumption. The methodology could however just as well be used on the other cavity types, the only modification would be to change some of the parameters. The β is in this context a measurement of the velocity of the particles, $v = \beta \cdot c$ where c denotes the speed of light.

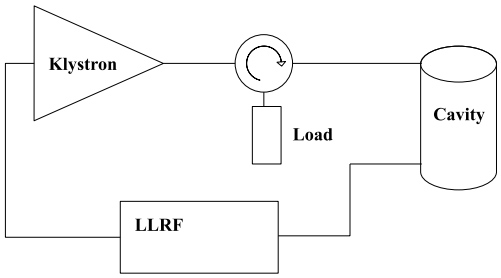

Figure 1.3 A subsystem of the accelerator showing the klystron, the circulator, the cavity and the LLRF system.

2. Theoretical background

2.1 Low Level Radio Frequency (LLRF) system

The LLRF system contains the controller with which the system can be affected. As mentioned before, the objective is to control the electric field of each cavity to follow given specifications of the amplitude and phase. To be able to do this, the field of the cavity is measured with a small antenna that is coupled in a way that gives a low impact on the field [3, Ch.4]. The measurements are then digitalized and sent to the controller. The controller uses the data, compares it to the references and calculates a new control signal that is D/A-converted and sent on to the klystron. How the control signal is calculated depends on the choice of controller and will be discussed in association with each of the two controller types used.

2.2 RF Cavity

An RF Cavity is a type of resonator that can be described as an LCR-circuit [12, Ch.3]. The inputs to the cavity are the current from the generator (klystron), I_g, and the beam current, I_b. This gives the total input $I = I_g + I_b = I_g - 2I_{b0}$, where I_{b0} is the DC component of the beam and the factor 2 occurs since the bunch length of the beam is short compared to the bunch spacing [12, Appendix A.4]. A schematic picture of the system, as seen from the cavity, is shown in Figure 2.1.

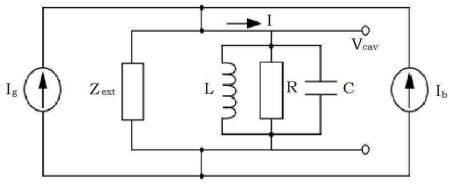

Figure 2.1 Schematic image of the system as seen from the cavity, adapted from [12]. The cavity consists of the LCR-circuit, I is the total input current and Z_{ext} is the external load as seen from the cavity.

The interesting parts in this application are the amplitude and phase, or real and imaginary parts, of the voltage in the cavity. The fast harmonic variations of the voltage due to the RF frequency are not as interesting as the slow changes of amplitude and phase over time. These slow changes are called the envelope of the signal (see Figure 2.2). The fast variations are separated from the slow changes in the following expressions of the signals:

$$\mathbf{V}(t) = (V_r(t) + iV_i(t)) \cdot e^{i\omega t} \quad (2.1)$$

$$\mathbf{I}(t) = (I_r(t) + iI_i(t)) \cdot e^{i\omega t} \quad (2.2)$$

where $\mathbf{V}$ is the voltage, V_r and V_i are the real and imaginary parts of $\mathbf{V}$, $\mathbf{I}$ is the current, with real and imaginary parts denoted I_r and I_i, and ω is the RF frequency.

If these signals are inserted to the differential equation of a driven LCR circuit, the equations for the cavity can be derived, and the result is shown in Eq.(2.3). For a detailed derivation of these equations, see [12].

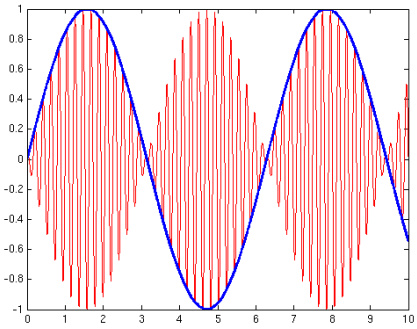

Figure 2.2 The envelope of the red high frequent signal is shown in the thick blue line.

$$\begin{aligned} \dot{V_r} + \omega_{1/2} V_r + \Delta\omega V_i &= R_L \omega_{1/2} I_r \\ \dot{V_i} + \omega_{1/2} V_i - \Delta\omega V_r &= R_L \omega_{1/2} I_i \end{aligned} \tag{2.3}$$

or in state space form with the state vector $x = \begin{pmatrix} V_r \\ V_i \end{pmatrix}$, and the input vector $u = \begin{pmatrix} I_r \\ I_i \end{pmatrix}$

$$\begin{aligned} \dot{x} &= \begin{pmatrix} -\omega_{1/2} & -\Delta\omega \\ \Delta\omega & -\omega_{1/2} \end{pmatrix} x + \begin{pmatrix} R_L\omega_{1/2} & 0 \\ 0 & R_L\omega_{1/2} \end{pmatrix} u \\ y &= \begin{pmatrix} 1 & 0 \\ 0 & 1 \end{pmatrix} x \end{aligned} \tag{2.4}$$

where

$$\omega_{1/2} = \frac{\omega_0}{2Q_L} \tag{2.5}$$

$$\Delta\omega = \omega_0 - \omega \tag{2.6}$$

$$\frac{1}{R_L} = \frac{1}{R} + \frac{1}{Z_{ext}} \tag{2.7}$$

and R and Z_{ext} are the impedances in Figure 2.1.

In the derivation of these expressions the second-order time derivatives of the voltage have been neglected, since they are comparatively small. It is also assumed that the resonance frequency of the cavity, ω_0, and the RF frequency, ω, are almost equal, and that the loaded quality factor, $Q_L \gg 1$. All parameters are listed in Appendix A.1.

2.3 Power generation

To be able to generate the power needed to reach the desired cavity voltages there are a few steps that need to be done. First of all, power from the wall socket is transformed to high DC voltage in a modulator. The high DC voltage is then transformed to an RF power in the klystron. This is needed since the cavity can not use the DC power directly. The RF power then needs to be transported to the cavity, this is done through waveguides and power couplings. The functionality of the different parts will now be described a bit more in detail [13].

Modulator

The modulator takes the alternating voltage from the electrical network and transforms it to a continuous high voltage. Since the RF system is pulsed, but the impact on the electrical network is preferably constant, the modulator uses capacitors that are continuously charged and then discharged when a pulse is wanted. Hence the modulator can be seen as a buffer for the voltage as well as a converter [13].

It is important to keep the high voltage signal as steady as possible during the pulse, but due to the discharging of the capacitors there will be a droop in the signal. There will also be some ripple in the signal due to, for example, resonance frequencies in the electrical circuit. The specifications of the modulator, relevant to this thesis, are listed in Appendix A.1. Ripple of higher frequencies than the one listed in A.1 are also present but at lower amplitudes and are not taken into account in this thesis.

Klystron

Klystrons are commonly used in radio transmitters and radars. They are also used in particle accelerators.

A klystron is itself a small particle accelerator. The physics of the klystron is shown in Figure 2.3. The electrons are bunched together by the RF field in the input cavity of the klystron. The voltage from the modulator makes the electron bunches gain more and more energy. This energy is then dissipated in the output cavity of the klystron and led on towards the RF cavity.

The klystron amplification is shown in the AM-AM curve in Figure 2.4 and AM-PM curve in Figure 2.5. These curves are the result of simulations made by the ESS RF group in the software AJ Disc [8]. AM stands for amplitude modulation while PM stands for phase modulation. The AM-AM curve shows the amplification in the klystron and the AM-PM curve shows the phase shift that the klystron gives rise to. As can be seen in Figure 2.4, there is a saturation of the output power. This occurs when the signal gets perfectly bunched. If the drive power is increased from that saturated drive power, the electrons start to pass each other and the bunching is no longer optimal. That is why the curve decreases for higher drive powers.

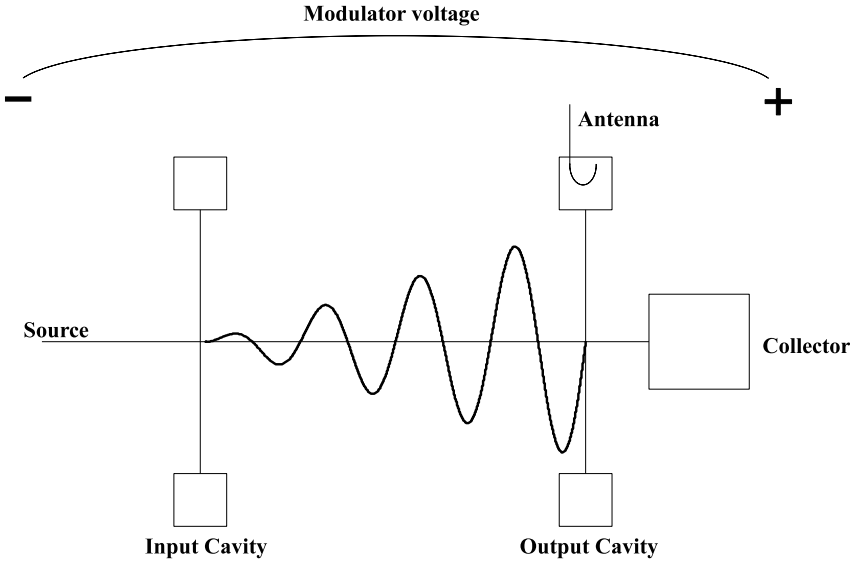

Figure 2.3 The physics of the klystron. Electrons from the electron source are bunched together by the drive power in the input cavity. The electron bunches are then accelerated by the modulator voltage. The output power from the klystron is lead out by an antenna from the output cavity.

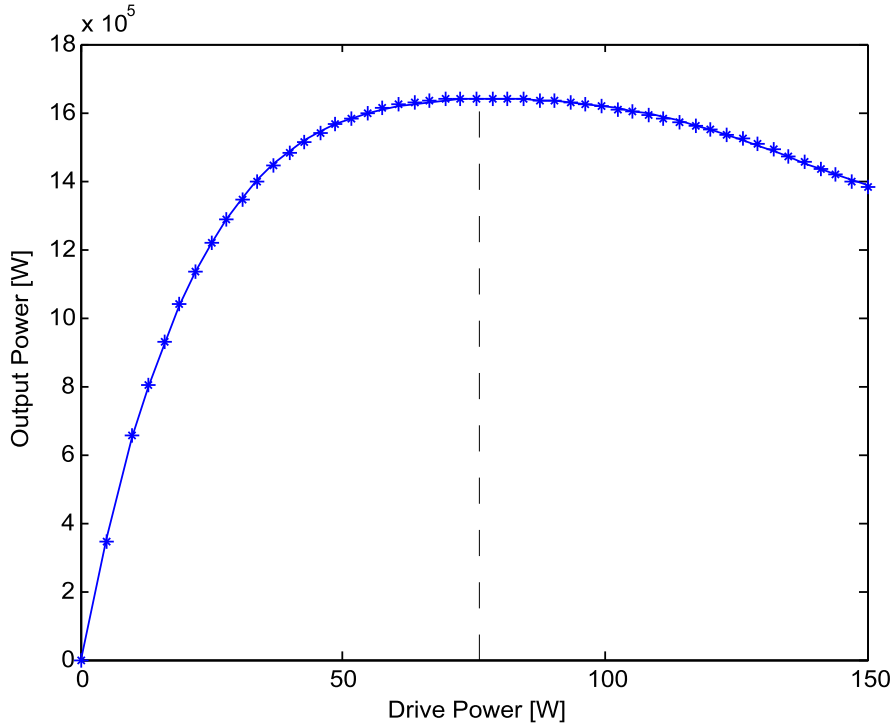

Figure 2.4 The AM-AM curve, where AM stands for amplitude modulation. This curve shows the amplification in the klystron. The saturation point is marked with a dotted line at the drive power 75.5 W. The stars show the data points received from [8]. The line is the resulting polynomial graph.

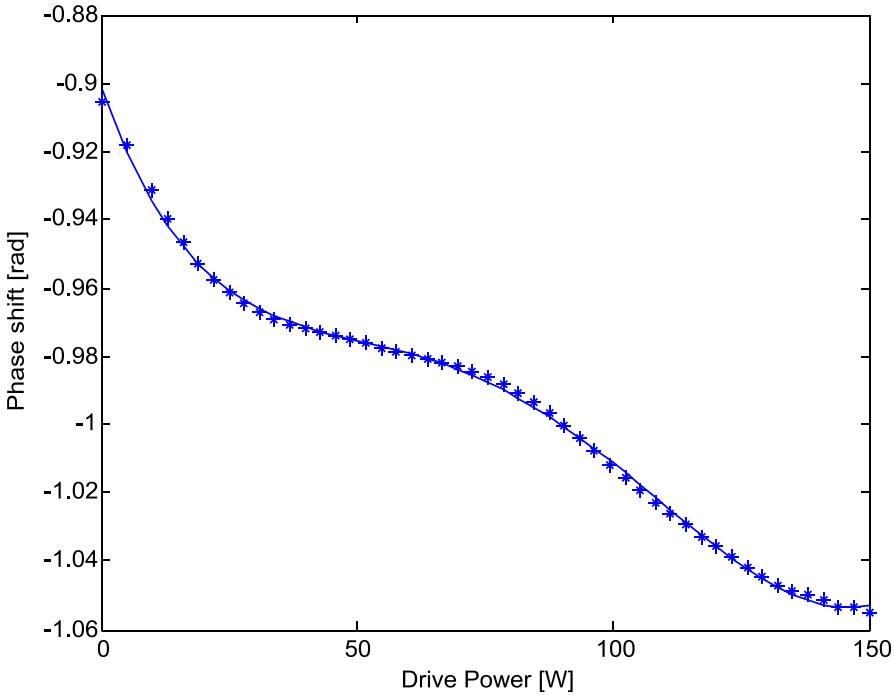

Figure 2.5 The AM-PM curve, where PM stands for phase modulation. This curve shows the phase shift in the klystron. The stars show the data points received from [8]. The line is the resulting polynomial graph.

Depending on the voltage from the modulator, the electron bunches will gain a different amount of energy while traveling through the klystron, which means that the AM-AM curve will be scaled differently in the y-direction. As a consequence of the scaling, the same output power can be achieved with a smaller modulator voltage if the operation area of the klystron can be moved upwards from the linear area towards the saturation point. This would increase the efficiency of the system and could drastically reduce the energy usage.

Waveguides and power coupling

The RF power is transported from the klystron to the cavity in a waveguide. The coupling between the waveguide and the cavity is important. The power needs to be inserted in such a way as to have significant influence on the field of the cavity. It also needs to make sure that the air from the waveguide does not enter the vacuum of the cavity [13].

If the impedances of the cavity and the klystron are not matched properly, some of the power (or voltage) will be reflected at the coupling. To get rid of the reflected waves, or at least to decrease them, the impedance of the cavity can be modified by detuning. Detuning occurs when the system is operated on another frequency than the resonance frequency of the cavity. The tuning angle ψ is the angle between the generator current and the generator voltage, and between the beam current and beam voltage [12, Ch.3].

2.4 Control design

Two different types of controllers will be used in this work. A PI controller, since that is what is normally used in similar processes today, and an MPC controller, since that is a more advanced, model based, controller that might improve the performance of the process. The ideas of the controllers will be described in this chapter, while the implementation of them will be described later on.

PI Controller

A PI(D) controller, Proportional Integral (Derivative) controller, is the most commonly used controller in industry. The input to the controller is the error e, which is given from $e = r - y$, where r is the reference and y the measured output. The control signal u is calculated according to the following formula:

$$u(t) = K\left(e(t) + \frac{1}{T_i}\int_0^t e(\tau)d\tau + T_d\frac{de(t)}{dt}\right) \tag{2.8}$$

where K, T_i and T_d are parameters that can be tuned by the user. To have a PI controller, i.e. no derivative part, as will be the case in this work, T_d is simply set to zero.

For more information on the functionality of a PI (or PID) controller read for example [1].

Model Predictive Control

An MPC controller calculates its control signal based on a model of the process. Under presumption that it has a good model, it can then use it to predict future values of the output. Hence the predictive part in the name. What it really does is to calculate the optimal solution, for a user specified prediction horizon p and control horizon m, to the cost function, Eq.(2.9). The cost function includes the reference values x^r, the state vector x and input vector u given as

$$x = \begin{pmatrix} V_r \\ V_i \end{pmatrix}, \quad u = \begin{pmatrix} I_r \\ I_i \end{pmatrix}$$

and the weight matrices Q_x, $Q_{\Delta u}$ and Q_u [2,10]. The weight matrix Q_u is set to zero as the value of the control signal u does not need to be punished as long as it stays within its boundaries.

$$\begin{aligned} J(u) = &\sum_{i=0}^{p}(x_{k+i} - x^r_{k+i})^T Q_x (x_{k+i} - x^r_{k+i}) \\ &+ \sum_{i=0}^{m}(\Delta u_{k+i})^T Q_{\Delta u}(\Delta u_{k+i}) + \sum_{i=0}^{m}(\bar{u}_j - u_{j_{k+i}})^T Q_u (\bar{u}_j - u_{j_{k+i}}) \end{aligned} \tag{2.9}$$

The solution to the optimization problem is the vector of m calculated control moves. The first control move is sent out to the system and the others are thrown away, then it all repeats itself in the next sample. The reason to throw away the following values and calculate them again is that you want to see if the result really became as expected. If the model is perfect and there are no disturbances acting on the process there would be no need to do this, then control moves could be calculated for the entire runtime. However, in reality there are no such things as perfect models and no disturbances, so some feedback is needed to make sure that the system really behaved as expected before calculating the next step.

The prediction horizon tells how far ahead the controller looks. The benefits of a long prediction horizon is that things like possible violation of constraints can be discovered in time and be prevented from happening. The drawback is that the number of calculations needed increase, which demands more time and computer power. There are some rules of thumb regarding the setting of prediction and control horizons. The prediction horizon should be larger than the process time delay d. At the same time the control horizon should be less than the prediction horizon minus the time delay [10, Ch.13].

3. Implementation

Since ESS will not be operational until 2019, all results and conclusions in this thesis are based on simulations made in Matlab/Simulink.

The particle accelerator will be a pulsed system with a repeating frequency of 14 Hz. The LLRF system and the klystron will be turned on at the start of each new cycle. After a specified time, t_{inj}, the proton beam injection will take place and it is important that the voltage of the cavity has reached its specified value when the beam arrives. The beam has a pulse length of 2.86 ms and after that the entire system is switched off until the start of the next cycle [3, Ch.1].

3.1 Overview of the Simulink model

As shown in the simplified picture in Figure 1.3, the LLRF system, the klystron and the cavity are connected in a feedback loop. In the real model there are some additional parts that need to be taken into account to make the simulation work as desired. An image of one of the Simulink models used is shown in Figure 3.1.

The first addition is to keep track of the time. Since the system is pulsed, the LLRF system, the klystron and the beam must be switched on and off at specific times. This is accomplished with the time generator block and the switch block in the Simulink model.

The next things added are the conversions between voltages, currents and powers that have to occur at the appropriate places. The cavity equation has a current as input and a voltage as output, while the controller only works with the voltages. The klystron curves are based on powers, and these conversions will be described more in Section 3.2. The conversion between the output voltage from the klystron to the input current of the cavity is $I_g = 2 \cdot V_g/R_L$, R_L being the loaded shunt impedance of the cavity, and the factor 2 appears as a consequence of the circulator [12, Ch.3].

The third item that is added is the transport delay that is inserted between the cavity and the controller. This is to make the model more realistic since there will be delays in the real system.

3.2 Klystron model

The klystron model is adapted from [9] and shown in Figure 3.2. The input signal to the klystron is the voltage divided into its real and imaginary parts. It is turned into amplitude and phase parts and the amplitude is converted to power as the curves are based on power signals. The conversion is made according to $P = V^2/(2 \cdot R)$. The factor 2 here appears since the power P is the root mean square value (P_{RMS}), while the voltage is the peak voltage $\hat{V}$. The $R = 50\ \Omega$ since it is the impedance of the transmission line between the LLRF system and the klystron.

The power signal is then sent through a filter (see Section **Filter** below) and after that it is saturated to make sure that the input to the curves is not higher than the saturated drive power. The output signal from the AM-PM curve is a phase shift which is added to the input phase and the phase shift from the modulator. The output signal from the AM-AM curve is multiplied with the amplitude factor from the modulator (see Section **Modulator** below). These two resulting signals are then converted back into voltage with a real and an imaginary part. The conversion from power to voltage on this side is $V_g = \sqrt{2 \cdot R_L \cdot P_{out}}$. The factor 2 occurs due to the same reason as before, but the impedance is now the loaded shunt impedance of the cavity R_L instead of the impedance of the transmission line.

The last feature in the klystron model is that a delay is added to the signal.

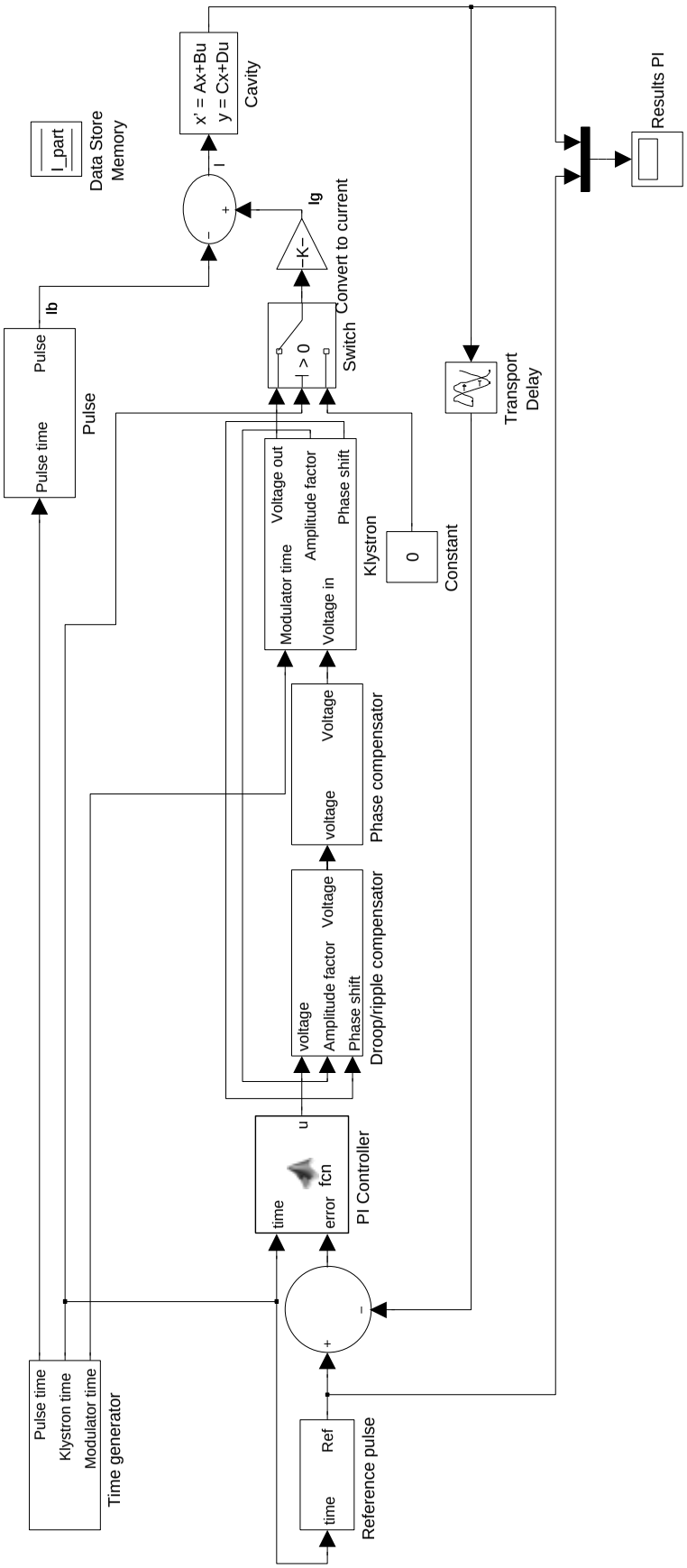

Figure 3.1 Simulink model of the system with the PI controller.

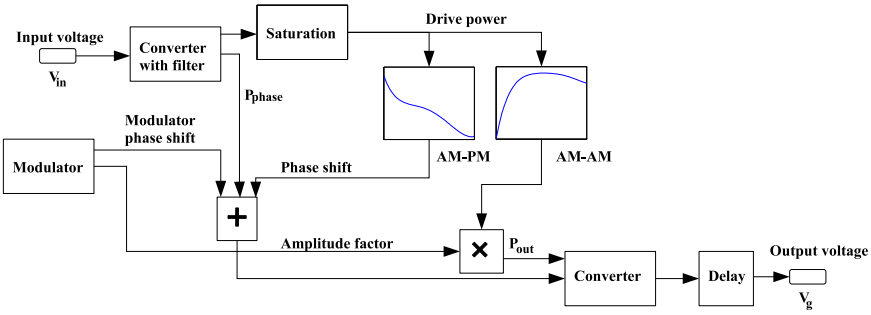

Figure 3.2 Schematic Simulink image of the klystron, adapted from [9].

Filter

The input signal, converted to power, passes a filter. Preferably frequencies around the RF-frequency, 704.42 MHz, should pass. Looking at small deviations around that frequency and shifting the zero to the RF-frequency, gives a lowpass filter. Originally the filter was a bandpass filter with bandwidth 1.75 MHz. Now, as a lowpass filter, the filter still has the same bandwidth. But looking only at the absolute value (the right side of the new zero) the bandwidth is halved and frequencies up to 0.875 MHz will pass, see Figure 3.3 [4].

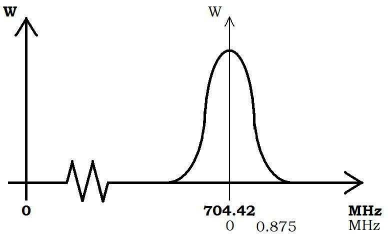

Figure 3.3 The filter in the klystron. Originally a bandpass filter, but effectively a lowpass filter.

Modulator

The modulator implementation gives a pulsed phase shift and amplitude factor. The phase shift begins at 0 and has a droop of 12°. There is also a sinus shaped ripple with amplitude 0.3% and frequency 1 kHz on it. The amplitude factor starts at 1 and has a droop of 1.25%, the ripple is the same as for the phase shift, see Figure 3.4 [4].

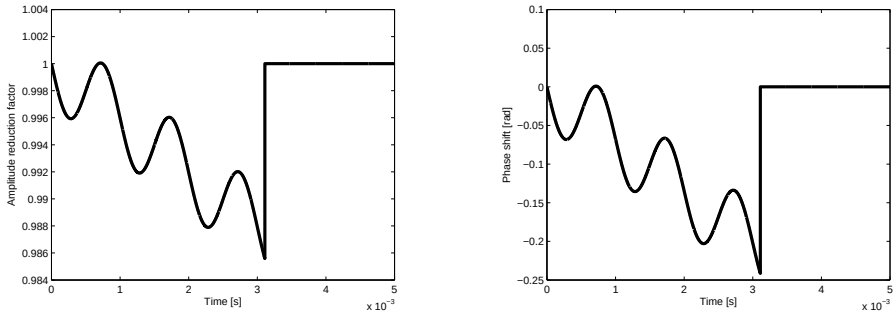

(a) (b)

Figure 3.4 The phase and amplitude changes due to modulator droop and ripple.

Curve generation

The polynomials, seen as lines in Figures 2.4 and 2.5, are produced using data from AJ Disc simulations. The data sets consist of points that can be seen as stars (*) in the respective figures. As the received data points only covered the drive power interval [10 W, 150 W], some fabricated points were added. It is not known what happens for a drive power lower then the specified interval, but for computational reasons two points extend the line towards zero drive power.

The Matlab command `polyfit` was used to adjust a line of the wanted order n to the submitted points. It returns coefficients for a polynomial on the form $a_1x^n + a_2x^{n-1} \cdots + a_nx$ where a_i are the coefficients and x is the input signal. These polynomials are then used in the AM-PM block and AM-AM block of the klystron implementation.

3.3 PI implementation

Due to some inconsistent results in the simulations with Simulink's built-in PI controller, the decision was made to implement our own PI controller to be able to track all the happenings.

The PI controller is implemented in discrete time where the integral has been approximated with a sum

$$u_k = K \cdot e_k + \frac{K}{T_i} \sum_{i=1}^{k} e_i \Delta t. \tag{3.1}$$

In the implementation the P part and the I part are calculated separately and then added together as $u_k = P_k + I_k$. The proportional part is calculated as $P_k = K \cdot e_k$. The integral part is saved after each step, and in the next step the integral part can be calculated as

$$I_k = I_{k-1} + \frac{K}{T_i} e_k \Delta t. \tag{3.2}$$

In the implementation the proportional gain K is called P and the integral gain K/T_i is called I.

Since there is a saturation in the klystron drive power the control signal is saturated. The saturation acts on the amplitude of the voltage, but the control signals are the real and imaginary parts of the voltage. Because of this complication the saturation is implemented as follows. First the amplitude of the original control signal is calculated

$$|V| = \sqrt{u_{re}^2 + u_{im}^2}. \tag{3.3}$$

Then, if this is bigger than the saturation limit, both u_{re} and u_{im} should be decreased as to keep the phase but decrease the amplitude. This is done by calculating a reduction factor

$$r_{fac} = \frac{|V|_{max}}{|V|} \tag{3.4}$$

and then multiplying it with the original control signals

$$\text{sat}(u_{re}) = u_{re} \cdot r_{fac} \tag{3.5}$$

$$\text{sat}(u_{im}) = u_{im} \cdot r_{fac}. \tag{3.6}$$

As always when there are saturations in the system there is a risk of a windup effect on the integral part of the controller. An anti-windup scheme is therefore implemented. If the saturated control signal differs from the original control signal, i.e. $\text{sat}(u) \neq u$, the integral part is recalculated as

$$I_k = \frac{1}{T_t}(\text{sat}(u_k) - P_k) \tag{3.7}$$

where T_t is a constant chosen in the implementation [1].

3.4 MPC implementation

The MPC-block is an existing block in the Simulink library, see [2]. There are three inputs to the block, the delayed cavity output, the reference signal and a measured disturbance, which in this case is the beam. There is also a saturation of the drive power. The saturation can not be implemented in the same way as in the PI controller, since the calculated control signal is not available when the limits are set in the existing MPC block. Instead, both the real part and the imaginary part are limited to the level of the saturation point mentioned in the klystron section in Chapter 2.3, transformed into voltage.

The starting point of the model to the MPC is the discretized state space equations of the cavity. Since the output from the MPC controller does not enter the cavity immediately, all the transitions in between also need to be part of the model. This is accomplished by modifying the discretized system B-matrix, B_{cav} to:

$$B_{modified} = B_{cav} \cdot \frac{2}{R_L}\sqrt{\frac{1}{R} \cdot R_L \cdot K_k}, \tag{3.8}$$

where K_k is a linear simplification of the klystron in the magnitude of the klystron amplification. The A and C matrices are the same as in the cavity.

The model also needs to be extended to handle the measured disturbance, the beam. The measured disturbance extends the input vector to

$$u = \begin{pmatrix} I_{g_r} \\ I_{g_i} \\ I_{b_r} \\ I_{b_i} \end{pmatrix} \tag{3.9}$$

which means that the B-matrix needs to be extended as well. This is done by $B = [B_{modified} \;\; B_{cav}]$. Since the beam enters the cavity directly there are no modifications to that part.

3.5 Phase compensator

As can be seen in Figure 2.5 the klystron causes a phase shift. To prevent unwanted effects of this phase shift a compensator block is added as a feed forward. What is done in the block is that the phase shift is precalculated from the AM-PM curve and added to the phase before it is sent in to the klystron. This way the total phase shift from the compensator block and the klystron is zero. The phase compensation has no impact on the amplitude.

3.6 Droop/ripple compensator

The droop and ripple of the modulator voltage, see Figure 3.4, affects the output as a disturbance that the controllers are not aware of. By measuring them and making a feed forward compensation of them the output could follow the references better. The droop and ripple enter the compensation block in the form of the phase shift, Δp, and the reduction factor of the amplitude, λ, that they gave rise to in the klystron in the previous sample. Inside the block the amplitude of the control signal is divided by the reduction factor and the phase shift is subtracted from the phase of the control signal. The modified control signal is the output of the block.

This compensator block does not cancel the entire effect, as the phase compensator block does. The total effect of the compensator block and the droop and ripple on the phase is

$$V_{phase}^{out} = V_{phase}^{in} - \Delta p_{k-1} + \Delta p_k, \tag{3.10}$$

which is good as long as $\Delta p_{k-1} \approx \Delta p_k$.

The amplitude out from the klystron if there had been no droop or ripple would be

$$|V_{out}| = f_{AMAM}(|V_{in}|) = K_{k_1} \cdot |V_{in}| \tag{3.11}$$

whereas the amplitude out from the klystron with droop and ripple and the compensation block is

$$|V_{out}| = f_{AMAM}\left(\frac{|V_{in}|}{\lambda_{k-1}}\right) \cdot \lambda_k = \frac{K_{k_2} \cdot |V_{in}|}{\lambda_{k-1}} \cdot \lambda_k \tag{3.12}$$

where $f_{AMAM}(V)$ represents the effect of the AM-AM curve of the klystron on the input V. Since that curve is not linear, i.e. $K_{k_1} \neq K_{k_2}$, they will not necessarily cancel each other out even if $\lambda_{k-1} \approx \lambda_k$.

4. Methodology

The objective of this thesis is to have a look at the klystron efficiency by experimenting with the AM-AM curve and to see if the MPC controller is a possible replacement of the PI controller by comparing the controllers.

To be able to do this, the control design and the parameters of the controllers will need to be decided. The methodology of these tests are described in Section 4.1 below. The robustness to setpoint changes will be tried according to the procedure described in Section 4.2. After that, the main test of the scaling of the AM-AM curve can be performed. The methodology of this test is described in Section 4.3.

The result of the experiments will be displayed graphically by plots from the simulation. Quantitative measurements will also be presented in some of the results. One measurement is the mean squared error e_{MS} calculated as

$$e_{MS} = \frac{1}{N} \sum_{k=t_0}^{t_0+N} |V_k - r_k|^2 \tag{4.1}$$

where t_0 is the first sample after the beam is injected, and N is the number of samples during the pulse. V_k is the voltage vector at sampling instant k, and r_k is the reference vector at that same sampling instant.

Another measurement is the elapsed time of the simulation. This is achieved by the commands `tic` and `toc` in Matlab. A problem with this time is that it depends on what other processes that are running on the computer during the simulation. To make it a slightly better measurement, the time value will be the mean value from 10 different simulation instances. Only significant differences in time will be discussed since small differences are in the scope of the variance.

4.1 Controllers

The process of finding the best PI controller and MPC controller for the system is divided into two parts. One part is to find the best control design, i.e., what additional blocks that are needed to make the performance as good as possible. The second part is to find the control parameters that give the best result. The two parts are interdependent, when a better set of parameters has been found the design tests are done again and vice versa.

Tests of the control design

In these tests the objective is to look at the effect of the compensator blocks that were discussed in Chapters 3.5 and 3.6. The tests are done by adding or removing the compensator blocks from the Simulink model, and are performed on both the PI model and the MPC model. The effect of having the beam as a measured disturbance in the MPC block will also be tested. The default version is to have the beam as a measured disturbance, hence the test consists of removing the measured disturbance.

Parameter settings

The controllers have a number of parameters that can be changed by the user. To find appropriate values of these parameters some testing has to be performed. The tests are done by varying one of the parameters while keeping the others constant and then evaluating whether the change led to an improvement or not.

In the PI controller the parameters available for tuning are the proportional gain P, the integral gain I, the sampling time T_s and the anti-windup time constant T_t. In the MPC controller the parameters to change are the prediction horizon p, the control horizon m, the sampling time T_s, and the weight matrices Q_x and $Q_{\Delta u}$.

4.2 Setpoint robustness

This test is done to see how robust the controllers are to changes in the reference values and pulse lengths. The test is based on the planned start-up phase of the accelerator.

During the accelerator's start-up, some smaller (lower amplitude) and shorter pulses than the usual pulse are used. If the regular pulse is used in the beginning and something is wrong with the accelerator, the consequences are devastating. Therefore these short, small pulses with less energy are used to make sure that everything is working as it should, to avoid damaging the accelerator.

The references are divided into 5 levels both in amplitude and in pulse length. First, there is a zero reference without any pulse. Then, there is a short, low pulse followed by short, higher pulses. When the correct amplitude is reached, the pulses are made longer until the regular pulse length is reached.

4.3 Klystron efficiency

The usual working area for the klystron lies around 0.9 MW in output power during the pulse since that is the power needed to remain stationary on the reference level, for calculations see Appendix A.2. With the original AM-AM curve this corresponds to a drive power of 16 W and is in the approximately linear part of the curve, see Figure 2.4. By scaling the curve the working area can be moved up and down on the curve and hence the klystron will get better or worse efficiency, see Section 2.3. Moving up on the curve means moving towards and into the non-linear area. Using different scaling factors between 0.5 and 2 gives an outlook on how the system will behave for the different areas of the curve. In this thesis it is assumed that the curve will scale linearly and thus keep the same shape independently of the scaling factors.

The AM-AM curves for the scaling factors 0.6 and 2 are shown in Figure 4.1. When the test is done on the MPC model, the scaling factor is also used to scale the approximative gain K_k discussed in Chapter 3.4.

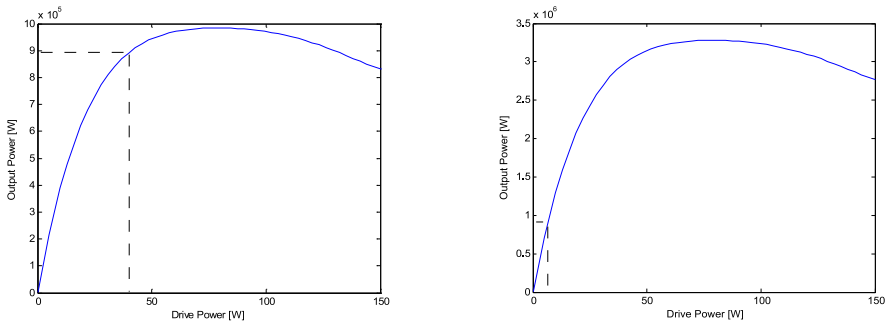

(a) (b)

Figure 4.1 The AM-AM curve scaled with a factor 0.6 in (a), and a factor 2 in (b). The output power 0.9 MW is marked in both pictures since that is the power needed to keep the cavity voltage stationary at the reference level, see Appendix A.2.

5. Results

Unless stated otherwise the parameters used in the following results are the ones given in Appendix A.3 for the PI controller and Appendix A.4 for the MPC controller. These are the parameter values that gave the best results during our tests.

The simulation parameters are listed in Appendix A.6.

5.1 Controllers

The result of a 0.3 second long simulation is shown in Figure 5.1. Here the pulsed operation of the system becomes visible.

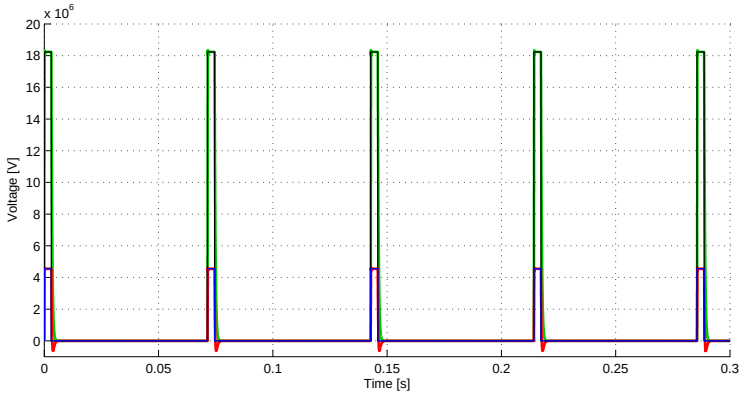

Figure 5.1 The real (green) and imaginary (red) part of the cavity voltage when running the PI model for a 0.3 second long simulation that shows five pulses.

The outputs for one pulse of the system for our final controllers are shown in Figure 5.2 for the PI controller and Figure 5.3 for the MPC controller. The figures show the real and imaginary parts of the cavity voltage, the amplitude of the cavity voltage with its specified limits of $\pm 1\%$, the phase of the cavity voltage with its specified limits of $\pm 1°$, and the drive power to the klystron. The quantified performance of the controllers is listed in Table 5.1.

The parameters and control design that are used in these figures are the ones that have given the best results in the tests of this section, they will be motivated by Figures 5.4 - 5.19 and Tables 5.2 - 5.8. The parameters are listed in Appendix A.3 and A.4.

Controller	e_{MS}	*Elapsed Time*
PI	$5.1869 \cdot 10^8$	2.9 s
MPC	$1.6307 \cdot 10^7$	2.5 s

Table 5.1 The quantified performance of the controllers. e_{MS} is the mean-square error and elapsed time is the simulation run time.

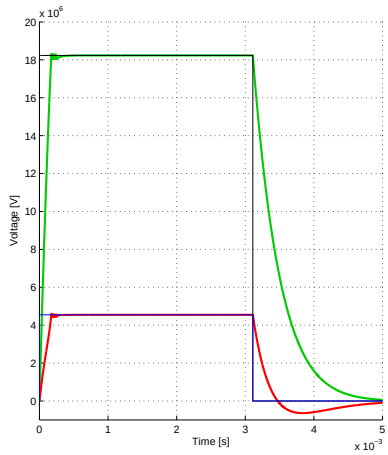

(a) Real (green) and imaginary (red) part of the cavity voltage. The black and blue lines are the corresponding reference values.

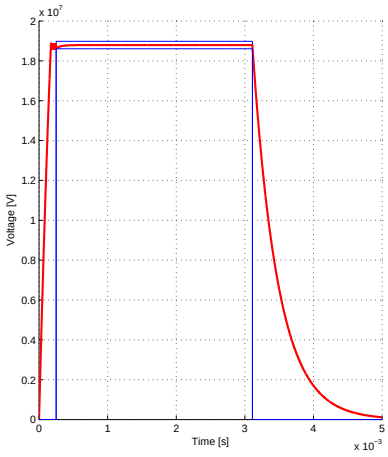

(b) Amplitude of the cavity voltage is shown in red, the limits in blue.

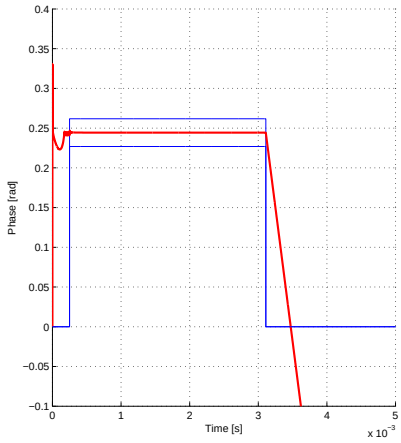

(c) The phase of the cavity voltage is shown in red, the limits in blue.

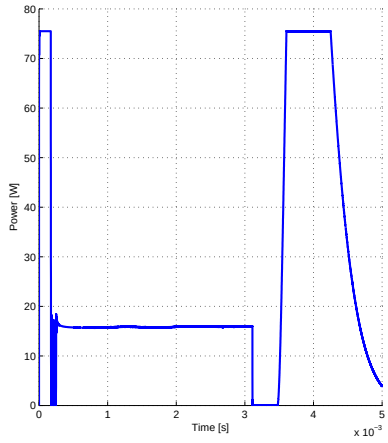

(d) Drive power to the klystron is shown in blue.

Figure 5.2 The results from the final PI controlled system.

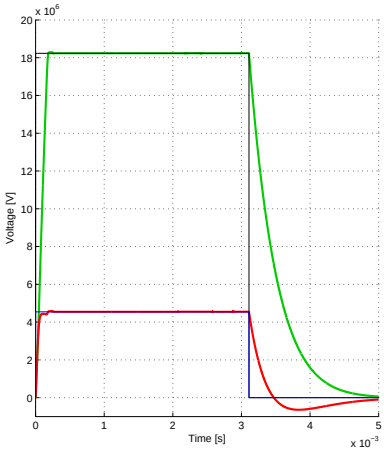

(a) Real (green) and imaginary (red) part of the cavity voltage. The black and blue lines are the corresponding reference values.

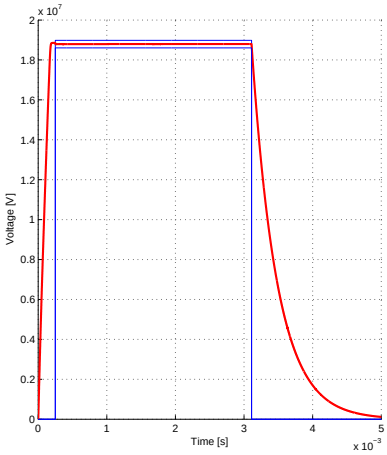

(b) Amplitude of the cavity voltage is shown in red, the limits in blue.

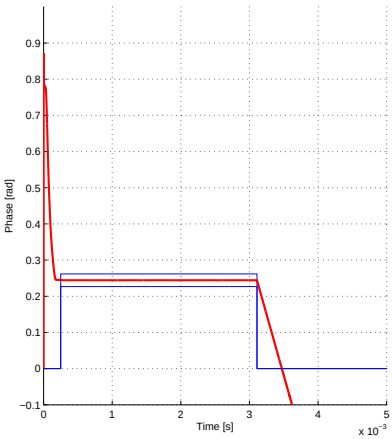

(c) The phase of the cavity voltage is shown in red, the limits in blue.

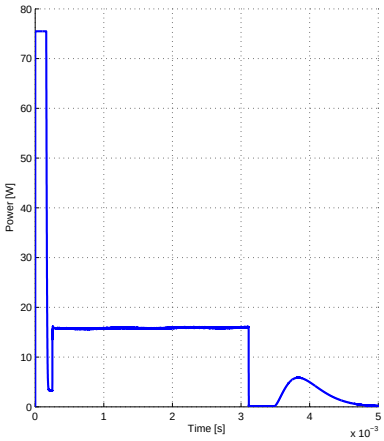

(d) Drive power to the klystron is shown in blue.

Figure 5.3 The results from the final MPC controlled system.

Tests of the control design

The real and imaginary outputs when no compensator block is used is shown in Figure 5.4. In (a) the result from the PI model can be seen. Before the pulse arrives there is a peak in the real part and a dip in the imaginary part. Both parts become oscillating when the pulse arrives, but lie around the reference voltage level. For the MPC model the result can be seen in (b). Before the pulse arrives, the behavior looks the same as for the PI model, but when the pulse arrives it gets a stationary error for both parts of the signal.

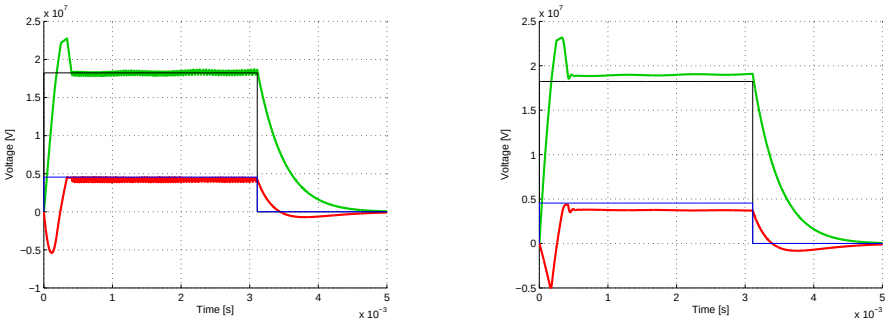

(a) (b)

Figure 5.4 The system run without the two compensation blocks. In (a) the PI model is used, and in (b) the MPC model is used. The green and the red line shows the real and imaginary parts of the cavity voltage, the black and blue lines are the corresponding reference values.

In Figures 5.5 and 5.6 the result with the phase compensator block is shown. In Figure 5.5 the signals look the same for the PI and the MPC systems, but when zoomed in (Figure 5.6) the differences are shown for the real parts.

The result when both the phase and droop/ripple compensators are connected is shown in Figure 5.7. This is used as default in both models.

The beam enters the MPC controller as a measured disturbance. The effect of this can be seen in Figure 5.8 where the beam is not a measured disturbance. Here the real part of the cavity voltage gets a stationary error during the pulse. That it only affects the real part is due to the fact that the beam is seen as a real constant current.

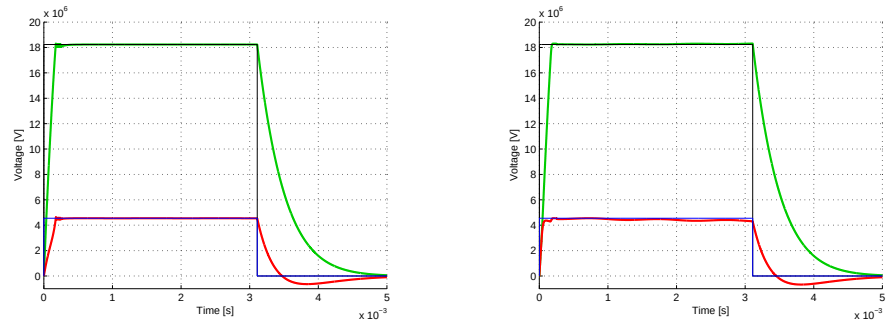

(a) (b)

Figure 5.5 The system run with the phase compensator, but without the droop/ripple compensator. In (a) the PI model is used, and in (b) the MPC model is used. The green and the red line shows the real and imaginary parts of the cavity voltage, the black and blue lines are the corresponding reference values.

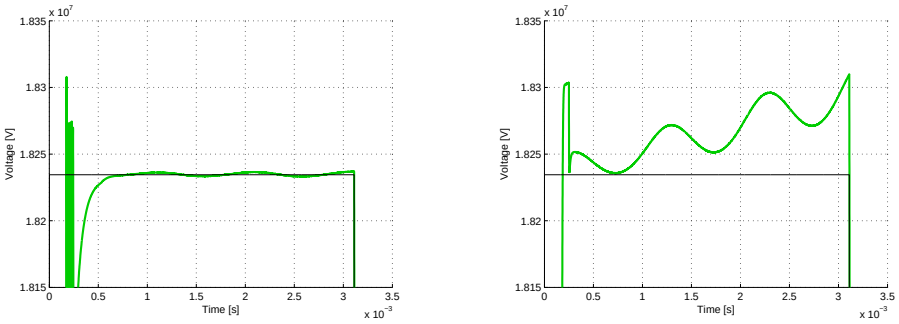

(a) (b)

Figure 5.6 The real part of the voltage zoomed in when the system has been run with the phase compensator but without the droop/ripple compensator. In (a) the system is run with the PI model, in (b) with the MPC model. The green line is the real part of the voltage and the black line is the reference value.

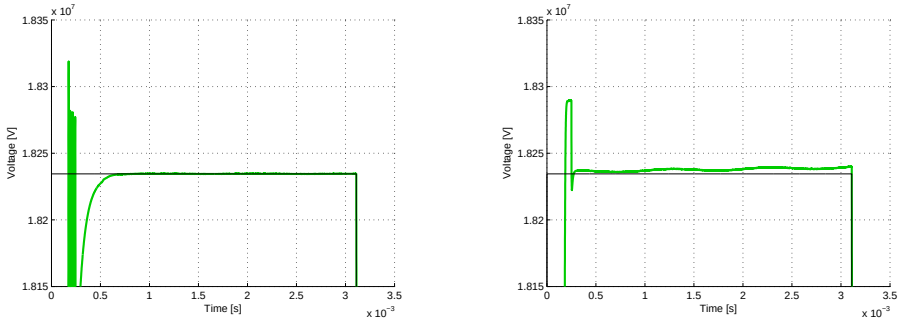

(a) (b)

Figure 5.7 The real part of the voltage in the cavity zoomed in. During simulation both the phase compensator and the droop/ripple compensator were connected. In (a) the system is run with the PI model, in (b) with the MPC model. The green line is the real part of the voltage and the black line is the reference value.

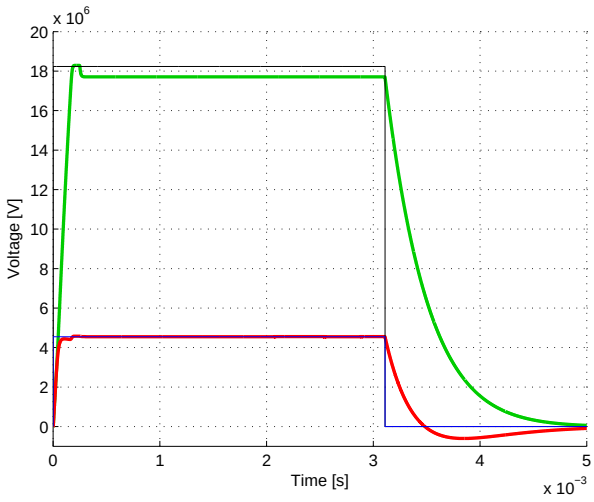

Figure 5.8 The real (green) and imaginary (red) part of the voltage when running the MPC model without the beam as a measured disturbance.

Parameter settings

PI controller

In the PI controller the control parameters P, I, T_s and T_t can be changed.

The results of varying the parameter P is shown in Table 5.2 and Figure 5.9. In Figure 5.9(a) the amplitude of the signal with its specification limits is shown when P is set to $3 \cdot 10^{-4}$, this gives rise to oscillations and the signal is below the lower amplitude limit in a lot of occasions. In Figure 5.9(b), P is instead set to 10^{-4}, the signal is under the lower limit in the beginning of the pulse, but is well inside the rest of the pulse time.

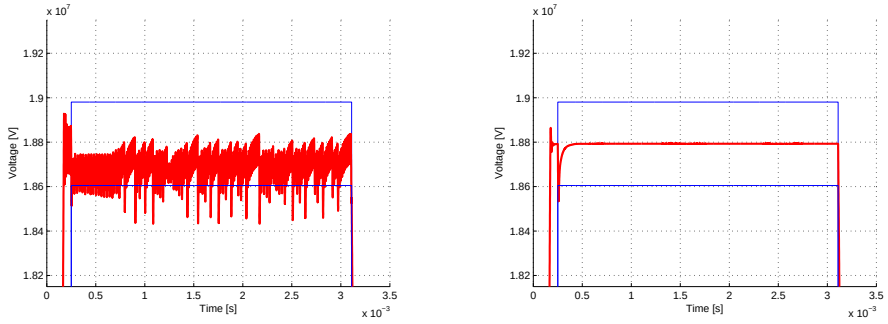

(a) (b)

Figure 5.9 The system run with the PI controller. The control parameter $P = 3 \cdot 10^{-4}$ is used in (a) and $P = 10^{-4}$ is used in (b). The amplitude of the cavity voltage is shown in red, the limits in blue.

P	e_{MS}	*Elapsed Time*
$1 \cdot 10^{-4}$	$5.1173 \cdot 10^{8}$	2.6 s
$2 \cdot 10^{-4}$	$5.1869 \cdot 10^{8}$	2.9 s
$3 \cdot 10^{-4}$	$1.8702 \cdot 10^{10}$	4.0 s
$1 \cdot 10^{-3}$	$3.2603 \cdot 10^{10}$	4.5 s
$1 \cdot 10^{-5}$	$3.2603 \cdot 10^{10}$	4.5 s

Table 5.2 Results of different values of P. Other parameters used have default values. e_{MS} is the mean squared error and elapsed time is the simulation run time.

The results of varying the parameter I is shown in Figure 5.10 and in Table 5.3. In Figure 5.10(a) I is set to 180. This gives an amplitude that is just outside the lower amplitude limit in the beginning. When I is set to 140, as shown in Figure 5.10(b), the signal is just inside the amplitude limits, though very close to the lower limit.

The results of varying the parameter T_s is shown in Figure 5.11 and in Table 5.4. The parameter T_s is in Figure 5.11(a) set to $3 \cdot 10^{-9}$ s. It can be seen that the amplitude of the signal is outside the lower limit in the beginning of the pulse. In Figure 5.11(b), T_s is set to $5 \cdot 10^{-10}$ s, this gives a similar result with the signal outside the amplitude limit in the beginning of the pulse.

The parameter T_t, which is a part of the anti-windup in the controller, has in Figure 5.12(a) been set to 1. This gives a signal that just about reaches the correct amplitude in time, and when the pulse arrives it has a dip outside the lower amplitude limit. The default value of T_t has been used in Figure 5.12(b) and here the amplitude stays inside the limits. The result for some other values of T_t is listed in Table 5.5.

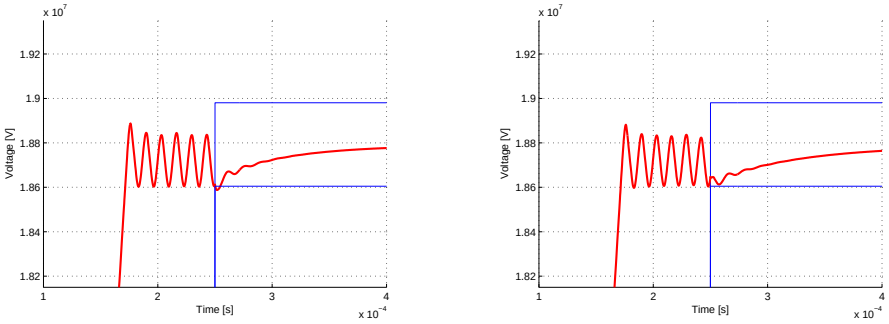

(a) (b)

Figure 5.10 The system run with the PI controller where the control parameter $I = 180$ in (a) and $I = 140$ in (b). The amplitude of the cavity voltage is shown in red, the limits in blue.

I	e_{MS}	*Elapsed Time*
140	$5.8754 \cdot 10^8$	2.7 s
150	$5.5687 \cdot 10^8$	2.7 s
160	$5.1869 \cdot 10^8$	2.9 s
170	$5.4805 \cdot 10^8$	2.7 s
180	$4.9152 \cdot 10^8$	2.7 s

Table 5.3 Results of different values of I. Other parameters used have default values. The default value is $I = 160$. e_{MS} is the mean squared error and elapsed time is the simulation run time.

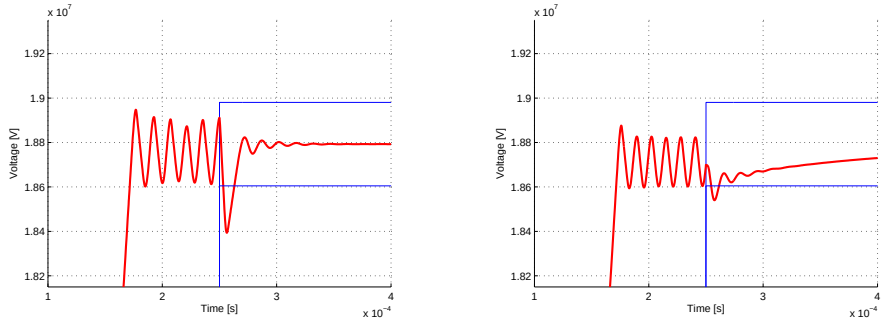

(a) (b)

Figure 5.11 The system run with the PI controller where the parameter $T_s = 3 \cdot 10^{-9}$ s in (a) and $T_s = 5 \cdot 10^{-10}$ s in (b). The amplitude of the cavity voltage is shown in red, the limits in blue.

T_s	e_{MS}	*Elapsed Time*
$1 \cdot 10^{-10}$ s	$5.7257 \cdot 10^9$	3.1 s
$5 \cdot 10^{-10}$ s	$1.0834 \cdot 10^9$	2.7 s
$1 \cdot 10^{-9}$ s	$5.1869 \cdot 10^8$	2.9 s
$3 \cdot 10^{-9}$ s	$1.4509 \cdot 10^9$	2.7 s
$1 \cdot 10^{-8}$ s	$4.6489 \cdot 10^{10}$	6.3 s

Table 5.4 Results of different values of T_s. Other parameters have default values. e_{MS} is the mean square error and elapsed time is the simulation run time.

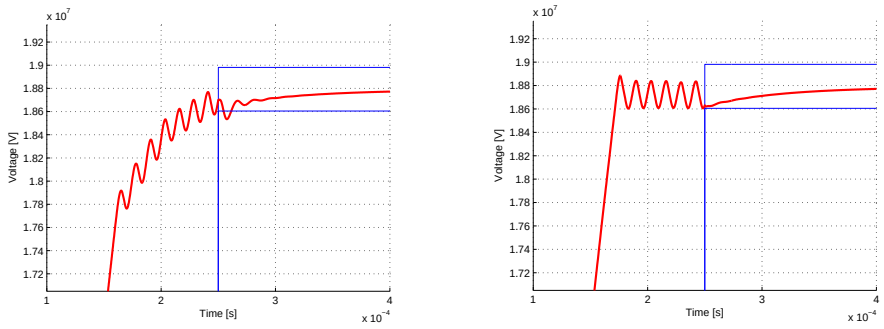

(a) (b)

Figure 5.12 Amplitude of the cavity voltage (red) of the system with the PI controller zoomed in on the beginning of the pulse. The parameter $T_t = 1$ in (a) and $T_t = 100$ in (b). The blue lines are the amplitude limits.

T_t	e_{MS}	*Elapsed Time*
1	$6.0879 \cdot 10^8$	2.9 s
10	$5.2294 \cdot 10^8$	2.8 s
50	$5.8986 \cdot 10^8$	2.7 s
100	$5.1869 \cdot 10^8$	2.9 s
150	$5.2589 \cdot 10^8$	2.7 s
200	$5.6656 \cdot 10^8$	2.7 s

Table 5.5 Results of different values of T_t. Other values have default values. e_{MS} is the mean square error and elapsed time is the simulation run time.

MPC controller

There are five parameters to tune in the MPC controller. The prediction horizon p, the control horizon m, the sampling time T_s, and the two weight matrices $Q_{\Delta u}$ and Q_x.

The tests of the horizons were performed with another set of weight matrices than the default ones. As can be seen in Figure 5.13 the default weight matrices combined with a control horizon $m = 3$ gives a choppy signal. To prevent the control signal from such quick variations in each control move, a higher weight on the input rate was added. The change to $Q_{\Delta u} = (10^5 \quad 10^4)$ and $Q_x = (1 \quad 1)$ gives the result in Figure 5.14. To give control horizons larger than 1 a fair trial, this set of weight matrices was used in the comparisons of the horizons.

The results of different prediction and control horizons are shown in Figures 5.15 and 5.16 and in Table 5.6. The short prediction horizon does not look far enough and gives an oscillating result. The long prediction horizon looks too far, and to not break the upper limit in the end it has to use a smaller control signal, and therefore does not reach the specified interval in time.

The results of different sampling times T_s are shown in Figures 5.17 and 5.18 and in Table 5.7. The prediction horizon needs to be adjusted to the sampling time since the prediction horizon is the number of sampling instances the controller looks ahead. Because of that the prediction horizon is also a listed parameter in Table 5.7. The value of the prediction horizon has its starting point in the default value $p = 15$ for $T_s = 1$ μs. This value could either be seen as a constant, or as the number of sampling units that is needed to look ahead of the delay of 2 μs plus thirteen steps more, or as the number of sampling units needed to look 15 μs ahead. One of these interpretations is what is used for the values of the prediction horizons when a shorter sampling time than the default one has been used.

The result from the tests with different weight matrices is shown in Table 5.8. In Figure 5.19 different weights have been added to each of the two outputs. When a higher weight is put on the real part, the imaginary part does not follow its reference in the beginning of the pulse. When a higher weight is put on the imaginary part the effect is not as visible since the real part is larger and hence affects the total cost function more.

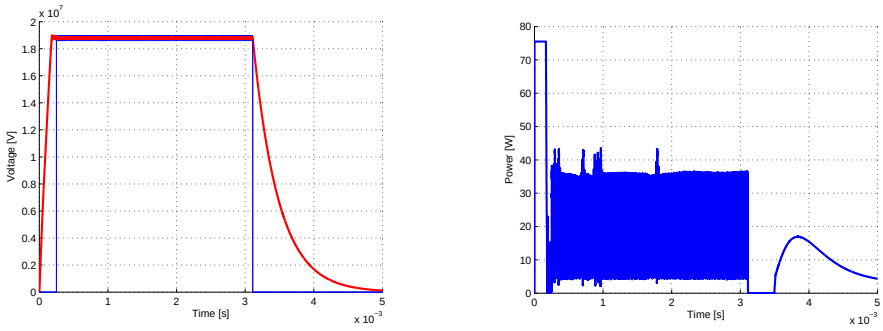

(a) (b)

Figure 5.13 The system run with the MPC controller. Our default weight matrices have been used with a control horizon $m = 3$. The resulting signal is very choppy which can be seen in the amplitude plot in (a), but is more prominent in (b) which shows the drive power to the klystron.

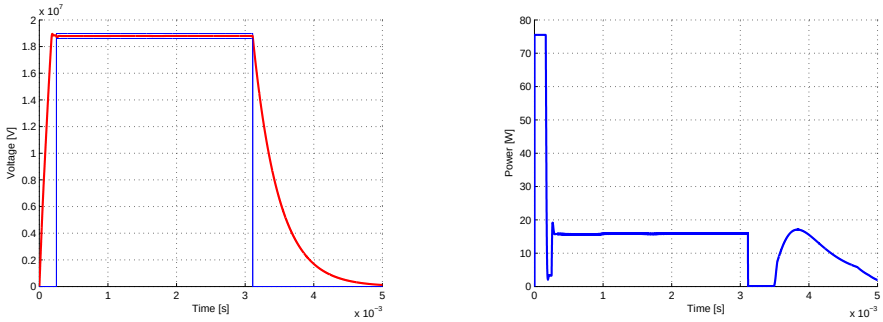

(a) (b)

Figure 5.14 The system run with the MPC controller. The set of weight matrices $Q_{\Delta u} = (10^5 \quad 10^4)$ and $Q_x = (1 \quad 1)$ is used with the control horizon $m = 3$. In (a) the amplitude of the cavity voltage is shown in red and the limits in blue. In (b) the drive power to the klystron is shown in blue. As can be seen, the control signal (drive power) does not vary so much since those variations are now punished by more weight.

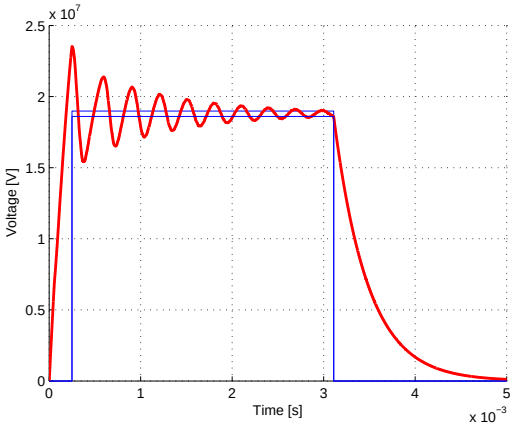

Figure 5.15 System run with an MPC controller with prediction horizon $p = 1$ and control horizon $m = 1$. The amplitude of the voltage is shown in red, and the limits are the blue lines.

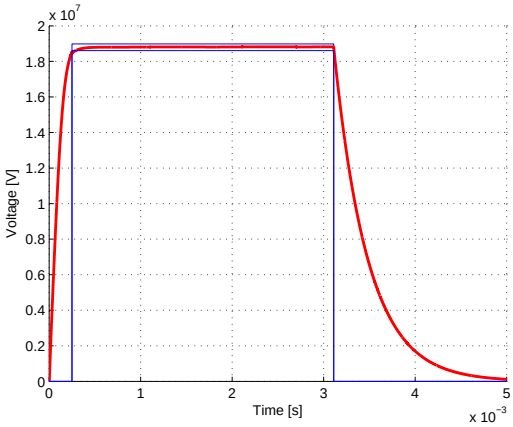

Figure 5.16 System run with an MPC controller with prediction horizon $p = 100$ and control horizon $m = 1$. The amplitude of the voltage is shown in red, and the limits are the blue lines.

Prediction horizon	*Control horizon*	e_{MS}	*Elapsed Time*
1	1	$1.4022 \cdot 10^{12}$	4.0 s
15	1	$4.5932 \cdot 10^{7}$	2.5 s
15	3	$1.4603 \cdot 10^{8}$	2.7 s
30	1	$7.7636 \cdot 10^{7}$	2.4 s
30	3	$6.8962 \cdot 10^{7}$	2.6 s
30	5	$1.6501 \cdot 10^{8}$	2.8 s
100	1	$2.4696 \cdot 10^{9}$	2.4 s
100	10	$1.6889 \cdot 10^{8}$	2.7 s
100	20	$2.5212 \cdot 10^{8}$	5.4 s

Table 5.6 Results of different prediction and control horizons. In these tests the set of weight matrices $Q_{\Delta u} = (10^5 \quad 10^4)$ and $Q_x = (1 \quad 1)$ has been used.

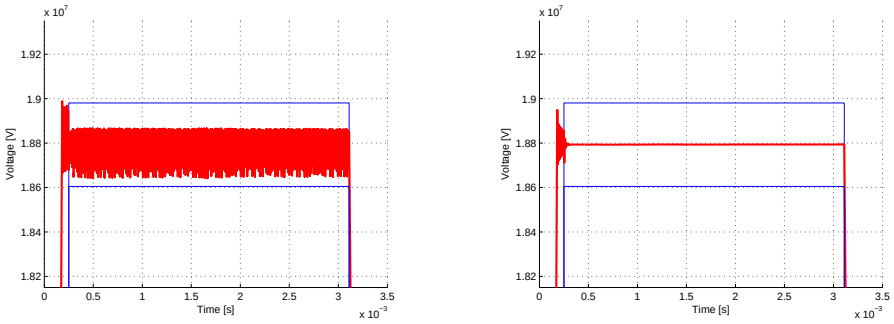

(a) (b)

Figure 5.17 System run with the MPC controller with a sampling time of 10^{-7} s. In (a) the prediction horizon $p = 15$, while in (b) the prediction horizon $p = 33$. The amplitude of the cavity voltage is shown in red, the limits in blue.

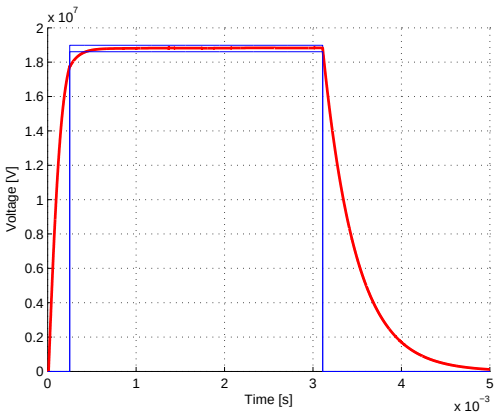

Figure 5.18 The system run with the MPC controller with sampling time $T_s = 10^{-5}$ s and prediction horizon $p = 15$. The red line is the amplitude of the cavity voltage and the blue lines are the limits.

Sampling time	*Prediction horizon*	e_{MS}	*Elapsed Time*
10^{-5} s	15	$2.5783 \cdot 10^{10}$	2.2 s
10^{-5} s	5	$2.1339 \cdot 10^{8}$	2.1 s
10^{-5} s	1	$3.3388 \cdot 10^{10}$	2.2 s
10^{-6} s	15	$1.6307 \cdot 10^{7}$	2.5 s
10^{-7} s	15	$6.0376 \cdot 10^{9}$	9.2 s
10^{-7} s	33	$1.0578 \cdot 10^{7}$	9.4 s
10^{-8} s	15	$3.1123 \cdot 10^{10}$	88.0 s
10^{-8} s	213	$5.6670 \cdot 10^{8}$	93.0 s
10^{-8} s	1500	$1.3081 \cdot 10^{7}$	443.0 s

Table 5.7 The MPC system where different sampling times and prediction horizons have been tested. e_{MS} is the mean-square error and elapsed time is the simulation run time.

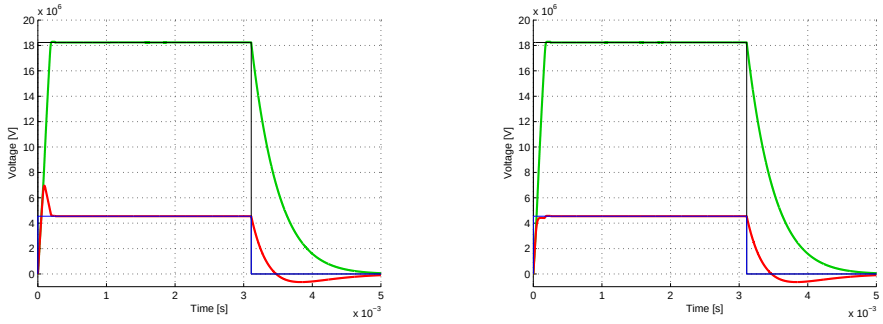

(a) (b)

Figure 5.19 The system run with the MPC model. In (a) the model is run with weight matrices $Q_{\Delta u} = (1 \quad 1)$ and $Q_x = (100 \quad 10)$. In (b) the same $Q_{\Delta u}$ has been used, but $Q_x = (10 \quad 100)$. The green and the red line shows the real and imaginary parts of the cavity voltage, the black and blue lines are the corresponding reference values.

$Q_{\Delta u}$	Q_x	e_{MS}	*Elapsed Time*
$(10^5 \quad 10^4)$	$(1 \quad 1)$	$4.5932 \cdot 10^7$	2.5 s
$(1 \quad 1)$	$(1 \quad 1)$	$1.6334 \cdot 10^7$	2.5 s
$(1 \quad 1)$	$(10 \quad 10)$	$1.6307 \cdot 10^7$	2.5 s
$(1 \quad 1)$	$(100 \quad 100)$	$1.6353 \cdot 10^7$	2.5 s
$(1 \quad 1)$	$(1000 \quad 1000)$	$1.6367 \cdot 10^7$	2.5 s
$(1 \quad 1)$	$(100 \quad 10\ )$	$1.7108 \cdot 10^7$	2.3 s
$(1 \quad 1)$	$(\ \ 10 \quad 100)$	$1.6677 \cdot 10^7$	2.6 s

Table 5.8 Different weight matrices $Q_{\Delta u}$ and Q_x has been tested on the MPC model. Other parameters are set to our default values. e_{MS} is the mean-square error and elapsed time is the simulation run time.

5.2 Setpoint robustness

The results from the test with different sized pulses are shown in Figure 5.20 for the PI model and in Figure 5.21 for the MPC model. As can be seen the PI model gets an irregular signal when the pulses are low in amplitude. The MPC model gets some stationary error for the lower pulses.

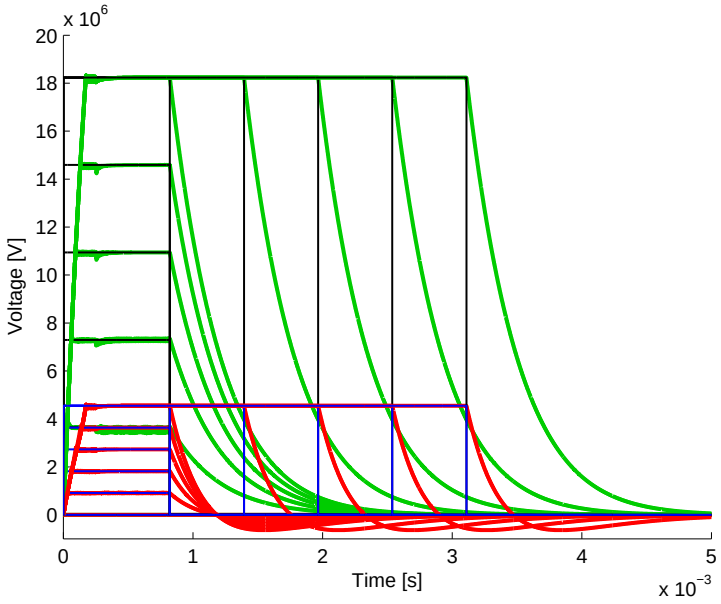

Figure 5.20 PI controlled system for pulses with different amplitudes and lengths. The voltage reference value is divided into five different hights and lengths plus a zero pulse. The black and blue lines are the real and imaginary parts of the voltage reference. The green and red lines are the real and imaginary parts of the voltage signal.

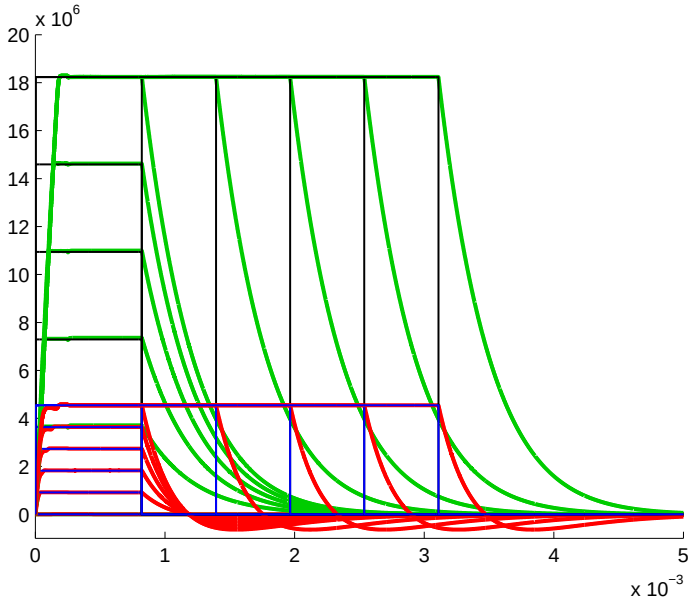

Figure 5.21 MPC controlled system for pulses with different amplitudes and lengths. The voltage reference value is divided into five different hights and lengths plus a zero pulse. The black and blue lines are the real and imaginary parts of the voltage reference. The green and red lines are the real and imaginary parts of the voltage signal.

5.3 Klystron efficiency

The results of the klystron efficiency test is shown in Table 5.9, and the result of the scaling factors 2 and 0.6 are shown graphically in Figures 5.22 - 5.24.

When running the default case (with a unit scaling factor) the signals are inside both the amplitude and phase limits, although close to the lower amplitude limit in the beginning of the pulse for the PI controller, see Figures 5.2 and 5.3. When moving down in the amplitude curve by multiplying with scaling factor 2 and 1.5, the PI controlled signal gets very oscillating as shown in Figure 5.22(a). With scaling factor 2 the MPC controlled system gets a signal that lies close to the higher amplitude limit, see Figure 5.23(a). As the scaling factor decreases the MPC system's signal decreases in amplitude and moves closer to the lower amplitude limit, and even passes it for scaling factor 0.6, see Figure 5.23(b). For the PI controlled system a scaling factor lower than the unit factor gives no oscillations, but a dip in the beginning of the pulse which goes outside the amplitude limits, see Figure 5.22(b).

If the internal model of the MPC is changed so that the K_k is not scaled linearly with the scaling factor 0.6, but instead looked up in the scaled AM-AM curve, the result is shown in Figure 5.24(a). In this figure there are no problems with staying inside the limits. As can be seen in Figure 5.24(b), the drive power to the klystron now lies around 45 W instead of around 16 W as in the default case, compare with Figure 5.3(d).

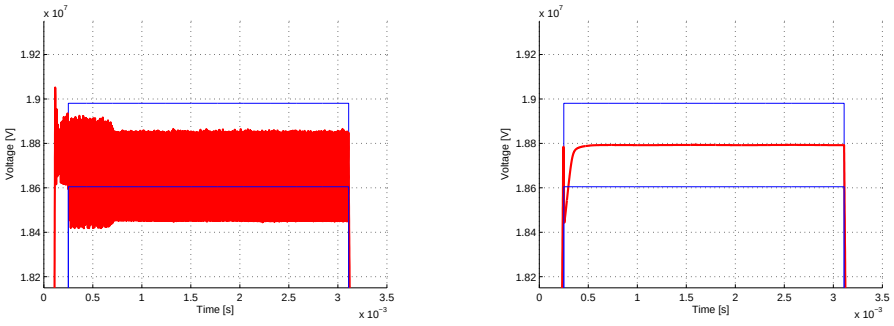

(a) (b)

Figure 5.22 The PI controlled system tested with differently scaled AM-AM curves. In (a) a scaling factor of 2 was used. In (b) a scaling factor of 0.6 was used. The amplitude of the cavity voltage is shown in red, the limits in blue.

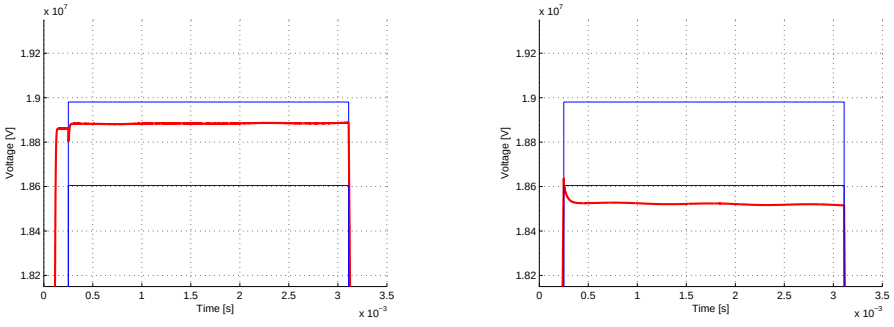

(a) (b)

Figure 5.23 The MPC controlled system tested with differently scaled AM-AM curves.. In (a) a scaling factor of 2 was used. In (b) a scaling factor of 0.6 was used. The amplitude of the cavity voltage is shown in red, the limits in blue.

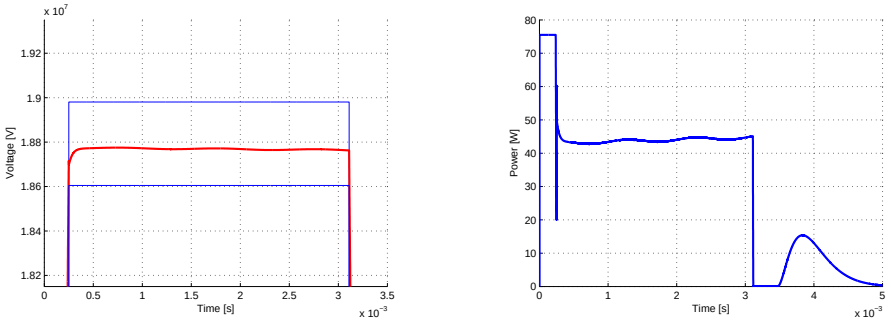

(a) (b)

Figure 5.24 Outputs of the system when run with an MPC controller. A scaling factor of 0.6 and $K_k = 2.2 \cdot 10^4$ has been used. In (a) the amplitude of the cavity voltage is shown in red, the limits in blue. In (b) the drive power to the klystron is shown in blue.

Scaling factor	*PI* e_{MS}	*MPC* e_{MS}	*Linear* K_k	*MPC* e_{MS}	*Looked-up* K_k	*MPC* e_{MS}
0.5	$3.93 \cdot 10^{12}$	$3.91 \cdot 10^{12}$	29000	$3.88 \cdot 10^{12}$	-	-
0.6	$2.72 \cdot 10^{9}$	$3.63 \cdot 10^{11}$	34800	$7.25 \cdot 10^{10}$	22000	$6.92 \cdot 10^{8}$
0.7	$9.37 \cdot 10^{8}$	$1.15 \cdot 10^{11}$	40600	$1.58 \cdot 10^{10}$	33000	$2.74 \cdot 10^{8}$
0.8	$5.11 \cdot 10^{8}$	$3.48 \cdot 10^{10}$	46400	$3.80 \cdot 10^{9}$	41000	$1.58 \cdot 10^{7}$
0.9	$6.79 \cdot 10^{8}$	$6.23 \cdot 10^{9}$	52200	$5.31 \cdot 10^{8}$	50000	$6.45 \cdot 10^{6}$
1.1	$5.39 \cdot 10^{8}$	$4.79 \cdot 10^{9}$	63800	$5.11 \cdot 10^{8}$	67000	$1.07 \cdot 10^{7}$
1.5	$1.27 \cdot 10^{10}$	$5.95 \cdot 10^{10}$	87000	$4.35 \cdot 10^{9}$	99000	$1.06 \cdot 10^{7}$
2	$4.71 \cdot 10^{10}$	$1.37 \cdot 10^{11}$	126000	$8.27 \cdot 10^{9}$	160000	$5.31 \cdot 10^{9}$

Table 5.9 Results from the scaling of the AM-AM curve. There are four different error measurements for each scaling factor. The first one is the error when the PI controller was used. The second one is when the MPC controller was used with an internal approximative gain $K_k = 58000$. The third version also uses the MPC controller, but this time with a linearly scaled internal gain. The last version is with the MPC controller as well, but this time the K_k has been looked up in the scaled AM-AM curve as the gain at the point where the output power of the klystron is equal to 0.9 MW. Since the curve never reaches 0.9 MW when the scaling factor 0.5 is used there are no values in the last column for that scaling factor.

6. Discussion

6.1 PI controller

The results of the default PI controller with the compensation blocks (see Figure 5.2) fulfill all requirements. The difficulty with the PI controller is to find a good set of control parameters. In this work trial and error was used to produce those. As can be seen in the results even a small change of one of the parameters often ends up in a system where the outputs falls outside the given specification limits. This indicates that it is not very robust to changes. Another thing worth mentioning about the control parameters is that as only one parameter at a time was changed, there might exist another set of parameters that would work just as well, or even better than the ones produced in this thesis.

In Figure 5.20 the model is tested in its ability to follow changing references. When the reference signal has a low amplitude the controller has some difficulties in following it, the signal starts to oscillate. This gets better when the pulses have higher amplitudes. A way to improve the performance on low pulses is to tune the control parameters for each amplitude.

The big problem in tuning the parameters is that there is a dip caused by the beam injection, and this dip often ends up below the limit. This could be solved by introducing some kind of feed forward control of the beam, like in the MPC where it enters as a measured disturbance. Since we know when and how it affects the system, that should not be very hard to do. However it has not been done in this thesis. What has been added though is the phase compensation block and the droop/ripple compensation block. As seen in the results (Figure 5.4 and Figure 5.5) the effect of the phase compensator is big, while the droop/ripple is not as significant. When the phase compensator block is added the large peak in the beginning and the oscillations disappear. When zoomed in on this curve though, as has been done in Figure 5.6 the droop/ripple effect can be seen. In Figure 5.7 the droop/ripple compensation is added and has reduced the error. However, the ripple can still be seen on the output which might be explained by the fact that the compensation is not perfect, as mentioned in Chapter 3.6.

6.2 MPC controller

The MPC controller with the compensation blocks and our default parameters gives a good result of controlling the system, as can be seen in Figure 5.3. There are no problems to stay within the limits in either phase or amplitude. The result is also quite good in the test of the different reference pulses, see Figure 5.21. However it is clear that the output is better for the higher pulses than the lower ones, this is since the K_k-value in the internal MPC model is adjusted to the klystron gain for the working point of the standard pulse. If the non-linearities of the klystron curve should be included in the internal MPC model, or the K_k would be changed according to different working points during the start-up phase, the control system would achieve better performance.

Regarding the setting of the parameters there are some additional remarks to be made. As already discussed in the result section there is a dependence between the weight matrices and the horizons, and also between the sampling time and the horizons. Hence the tuning can not really be done for one parameter at a time. The weight of the input rate $Q_{\Delta u}$ affects how much variation that is allowed in-between two control moves. In our default set of parameters the control horizon is set to $m = 1$, which reduces the significance of $Q_{\Delta u}$ since only one control move is performed in each

calculation of the cost function. Because of that it is possible to have a higher weight on the output signal than on the input rate which explains the default values of the weight matrices, however as can be seen in Table 5.8 the difference in performance is not very large for different values of Q_x.

When it comes to the sampling times, the prediction horizon needs to be adjusted to the sampling time. The default value of $T_s = 10^{-6}$ is not the best performing alternative in Table 5.7. Shorter sampling periods with longer prediction horizons can give better results. The problem with those is that they need to make much more computations which takes longer time, and since the default one has no problem in fulfilling the limit specifications there is no need to increase the complexity of the optimization problem at this stage.

The default horizon values have the best performance in Table 5.6. As stated in Section 2.4 the prediction horizon at least needs to be larger than the time delay of the system, and it is clear in Figure 5.15 that a too short prediction horizon does not give a good result. As seen in Figure 5.16 a too long prediction does not give a good result either, at least not in combination with a short control horizon, since it then does not reach the specified values quick enough. The problem in this case is that when $m = 1$ the controller can not set a sufficiently high control signal to reach the specifications, since the optimization is based on the assumption that the control signal does not change during the prediction horizon and a high signal would then lead to a much too high output in the end. As can be seen in Table 5.6 the long prediction horizon gives a better result if the control horizon is also increased. If the control horizon is increased too much though, the result gets worse again.

The added compensation blocks have more or less the same impact on the MPC as they had on the PI controller. The phase compensation gives a clear improvement, while the droop/ripple compensation is not as significant but still an improvement. Another thing that is added to the MPC model is the measured disturbance. Without it, as in Figure 5.8, the real part of the voltage gets a stationary error. The reason why the MPC controller handles this worse than the PI controller is that it is more dependent on its internal model. If the model differs too much from the reality the MPC controller will have problems. That is also probably the cause to why the droop/ripple shows much more in the output from the MPC controller than from the PI controller.

6.3 Klystron efficiency

As can be seen in Figure 5.22(a), the PI controller has some problems with the scaling factor 2. This is not a consequence of the non-linearity since a scaling factor larger than unity moves the working area even further down to the linear area of the klystron. Instead it is due to the fact that the klystron gain in this area is higher than before, which gives the same effect as if the parameter P would be increased. As listed in Table 5.9 the klystron gain at the working point 0.9 MW when the scaling factor 2 is used is approximately $1.6 \cdot 10^5$ compared to $5.8 \cdot 10^4$ in the non-scaled case. This problem is solved by reducing the parameter P. But we do not want to go down in efficiency but up, so the most interesting curves are the ones for a scaling factor smaller than one.

The PI controlled system in Figure 5.22(b) seems to handle the scaling factor of 0.6 quite good, except for the dip in the beginning of the pulse. This dip might be removed by fine-tuning of the control parameters for this specific klystron curve, or by introducing a feed forward control of the beam as previously discussed. The MPC controlled system with a linearly scaled K_k, shown in Figure 5.23(b), ends up below the specification limits. This is due to the not so good scaling of the K_k. When a more accurate value has been used as in Figure 5.24(a) the result is very good. Deciding the K_k for the klystron curve that is to be used is not a problem and hence this result shows that it is clearly possible to increase the klystron efficiency with the MPC controller. The results listed in Table 5.9 show that the MPC with manually

looked up values of K_k gives reasonable results for all scaling factors. There are even some that give a better result than the default version. This is probably a sign that the K_k found for these scaling factors are more correct than the one approximated for the non-scaled case.

As can be concluded from these results there is no problem with increasing the klystron efficiency when the MPC controller is used as long as there is an appropriate internal model in the MPC. The PI controller can probably be used as well, but then some modification of the parameters or the control design needs to be done.

A remaining question is then how much the klystron efficiency could be increased. It is not wanted to push it too far since it would be very sensitive to disturbances if there are no margins at all. A scaling factor of 0.6 would increase the efficiency with a factor $1/0.6 \approx 1.66$, which of course would be very good. As can be seen in Figure 5.24(b) the drive power to the klystron is quite high, but there is still some extra power to put in if needed. If the scaling factor would be reduced further, the point would soon be reached when the power is not sufficient to get the voltage up to the specified value in time before the beam arrives. That would be solved by increasing the injection time but then the system will be running for longer time which demands more energy. If going as low as for example 0.5 there would not be enough power to stay at the reference values when the beam arrives no matter what is done, hence that is not an option.

6.4 Additional remarks

In this thesis some comparisons between the time consumption of the PI controller and the MPC controller have been made, but no effort has been put into trying to increase the efficiency of the algorithms. If the controllers derived here should be used in reality they need to be implemented in a more efficient way. As can be seen in the tables the elapsed time of the simulations (≈ 2.5 s) is much longer than the simulated time (0.005 s). When the control algorithms is run from saved values and separated from the rest of the simulation the running time is decreased to around 0.5 s. This is still a hundred times too slow to be able to run it in real time.

The system is likely to have some measurement noise and there may also be some variation in the process parameters. How these disturbances would affect the result has not been investigated. Intuitively we think that there might be a need to decrease the sampling time to be able to handle those things properly. The built-in disturbance models in the MPC block might also be of help if set in a good way.

There have been some problems with the existing Simulink blocks. As mentioned before the choice was made to implement our own PI controller to get better insight in what really happened. All saturation blocks were also replaced by simple `if`-statements which reduced former problems with too many consecutive zero crossings and decreased the computation time significantly. There was also a wish to replace the MPC block by a self-implemented one, but there was no time for implementing this. Some issues with the MPC block was discovered. The possibility of having a non-linear internal model would improve the results a lot. The insight into the built-in disturbance and noise models were not very good and sometimes led to problems with the internal state estimator that could not be constructed. There is also the problem with the saturation limits that could not be set in an appropriate way since we had no access to the manipulated variables in the setting of the saturation limits. All in all, there were a lot of things that we would have liked to be able to do differently and maybe at least some of those things could be achieved with a self-implemented MPC block.

7. Conclusions

In this thesis a PI controller and an MPC controller have been compared in their ability to control the electric field of the cavities in ESS's particle accelerator. The possibility to increase the efficiency of the klystron has also been investigated.

Both the PI and the MPC controller give satisfying results in normal operation. The MPC relies a lot on its internal model, therefore it is crucial to have a good one. But when the model is good it feels more robust to changes in for example setpoint values than the PI controller. The most important improvement to the MPC controller would be a way to model the non-linear klystron gain properly in the MPC internal model.

The PI controller behaves well when a good set of control parameters is used. The problem is to find these parameters. It can be a very time consuming process. The most important improvement to the PI model would be to add a feed forward control of the beam.

The klystron efficiency could be increased with the MPC controller, and probably with the PI controller as well. How much it could be increased is a compromise between how much margin to the maximum power that is wanted, and how much energy that would be saved.

8. Future work

To improve the results given in this thesis, and be able to use them on the real process, there are some issues to consider.

First of all the algorithms need to be implemented more efficiently to be able to run the process in real time. If the PI controller would be chosen to work with, feed forward control of the beam should be implemented. If the MPC controller would be chosen, it might be worth the effort to make a new implementation of it to have full control of, and full insight into, its functionality.

Another thing that needs to be done is to replace the simulated AM-AM curve and AM-PM curve to the curves for the actual klystrons that are to be used in ESS.

9. Bibliography

[1] K. J. Åström and R. M. Murray. *Feedback Systems: An Introduction for Scientists and Engineers*. Princeton University Press, Princeton, NJ, 2008.

[2] A. Bemporad, M. Morari, and N. L. Ricker. *Model Predictive Control Toolbox – User's Guide*, 2011.

[3] ESS Editor: S. Peggs. *ESS Conceptual Design Report*. European Spallation Source, February 2012. ESS-2012-001.

[4] A. J. Johansson, ESS, 2012. Personal Communication.

[5] Editor-in-chief: R. Eriksson, ESS. *ESS Accelerator homepage*. http://ess-scandinavia.eu/linac. 2012-05-30.

[6] Managing Editor: Dr C. Vettier, ESS. *Neutrons and Health*, July 2008.

[7] Managing Editor: Dr. Vettier, ESS. *Neutrons for Science*, June 2009.

[8] S. Molloy, ESS, 2012. Personal Communication.

[9] T. Poggi et al. ESS-Bilbao, RF Systems Group. *Modelling, control design and simulation of a klystron amplifier at ESS-Bilbao*. LLRF Workshop, DESY, Hamburg, Germany, 2011.

[10] R. Johansson. *Predictive and Adaptive Control*. Lund University, Dept. Automatic Control, 2011. Chapter 13.

[11] S. Werin, MAX-lab. *Accelerator Technique*. Lund, Sweden, 2006. 2.5th edition.

[12] T. Schilcher. *Vector Sum Control of Pulsed Accelerating Fields in Lorentz Force Detuned Superconducting Cavities*. PhD thesis, Universität Hamburg, Fachbereichs Physik, 1998.

[13] M. Vretenar. Radio frequency for particle accelerators - evolution and anatomy of a technology. In R. Bailey, editor, *Proceedings of the CAS-CERN Accelerator School: RF for accelerators*, number CERN-2011-007 in CERN Accelerator School, pages 1–14, Ebeltoft, Denmark, 8-17 June 2011.

A. Appendix

A.1 ESS Parameters for elliptical cavity high β

- $\beta = 0.9$
- Amplitude reference = 18.792700 MV
- Phase reference = 13.99996089°
- Amplitude limits = ±1%
- Phase limits = ±1°
- Maximum cavity fill time $t_{fill} = 250$ μs
- RF frequency $f = 704.42$ MHz
- RF frequency $\omega = 2\pi f$
- Tuning angle $\psi = 14°$
- Loaded quality factor $Q_L = 820 \cdot 10^3$
- Resonance frequency $\omega_0 = \omega + \frac{\omega \cdot tan(\psi)}{2Q_L}$
- $\frac{r}{Q} = 477\ \Omega$
- $R_L = \frac{r}{Q} \cdot \frac{Q_L}{2}$
- Pulse length = 2.86 ms
- Pulse frequency = 14 Hz
- Time delay = 2 μs
- $I_{b0} = 50$ mA
- $I_b = 2I_{b0}$
- Modulator pulse length = 3.5 ms
- Modulator droop amplitude = 1.25%
- Modulator droop phase = 12°
- Modulator ripple amplitude = 0.3%
- Modulator ripple frequency = 1 kHz

A.2 Calculation of necessary klystron output power

To remain stationary at the reference level the following equation needs to be fulfilled

$$0 = \dot{x} = A \cdot x_{ref} + B \cdot u$$
$$\Updownarrow$$
$$u = -B^{-1} \cdot A \cdot x_{ref}.$$

The input current to the cavity, u, is not only the generator current u_g but includes the input from the beam, u_{beam} as well. To get the needed generator current the latter one needs to be subtracte.

$$u_g = u - u_{beam}.$$

To find the necessary output power of the klystron the conversions between the klystron and the generator current is needed

$$|u_g| = \sqrt{P_{out} \cdot R_L \cdot 2} \cdot \frac{2}{R_L}$$
$$\Updownarrow$$
$$P_{out} = \frac{\left(\frac{|u_g| \cdot R_L}{2}\right)^2}{2 \cdot R_L} \approx 0.9 \text{ MW}.$$

A.3 Default values of PI parameters

- Sampling time, $T_s = 10^{-9}$ s
- Proportional gain, $P = 2 \cdot 10{-}4$
- Integral gain, $I = 160$
- $T_t = 100$
- $t_{inj} = 250\ \mu s$

A.4 Default values of MPC parameters

- Sampling time, $T_s = 10^{-6}$ s
- Prediction horizon, $p = 15$
- Control horizon, $m = 1$
- Approximative linear gain of the klystron, $K_k = 58000$
- Weight matrices, $Q_{\Delta u} = (1\ 1)$, $Q_x = (10\ 10)$
- Noise model: $\tilde{A} = \tilde{B} = \tilde{C} = \begin{pmatrix} 1 & 0 \\ 0 & 1 \end{pmatrix}$, $\tilde{D} = \begin{pmatrix} 0 & 0 \\ 0 & 0 \end{pmatrix}$
- $t_{inj} = 250\ \mu s$

A.5 Computer and software specifications

- Linux version 3.3.6-3.fc17.x86_64
- Processor: Intel(R) Core(TM) i7-2600 CPU @ 3.40GHz
- Matlab version: Matlab R2011a (64-bit)

A.6 Simulation parameters

- Solver type: Variable-step
- Solver: ode45 (Dormand-Prince)
- Max step size: 1e-6
- Min step size: auto
- Initial step size: auto
- Relative tolerance: 1e-3
- Absolute tolerance: auto
- Shape preservation: Disable all
- Number of consecutive min steps: 1
- Time tolerance: $10 \cdot 128 \cdot eps$ where $eps = 2.2204e - 16$
- Number of consecutive zero crossings: 1000

A.7 Simulink models and code

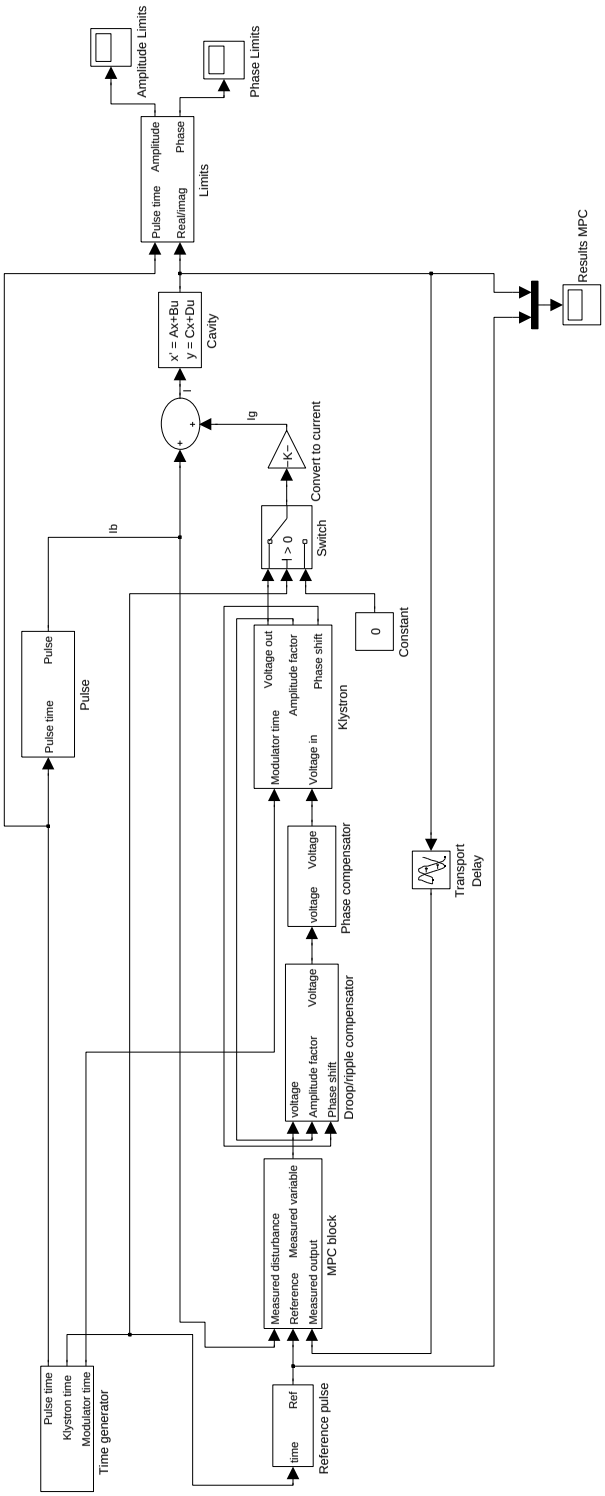

Figure A.1 The MPC Simulink model with shown scopes for the amplitude and phase limit curves.

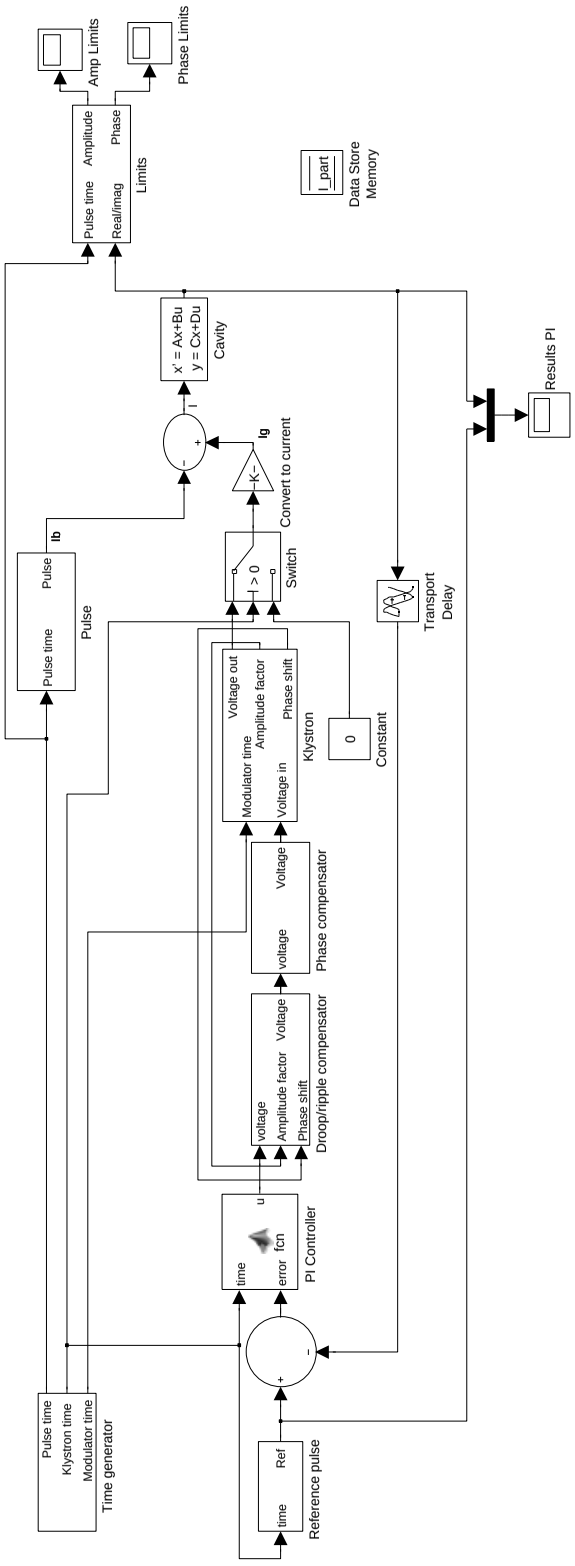

Figure A.2 The PI Simulink model with shown scopes for the amplitude and phase limit curves.

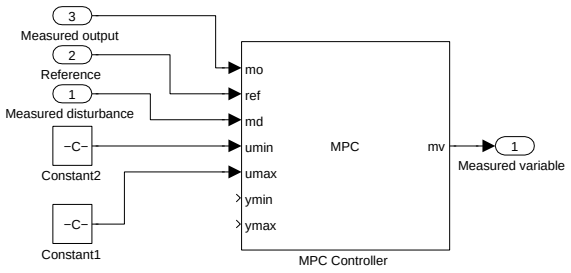

Figure A.3 The MPC Simulink block.

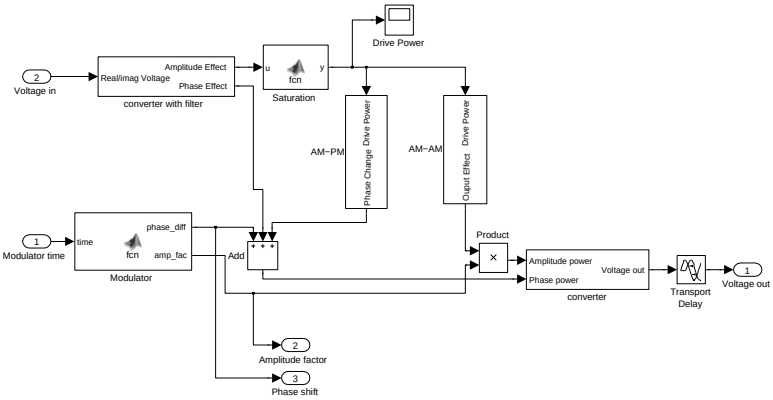

Figure A.4 The klystron model with shown scope for the drive power.

```
function [phase_diff, amp_fac] = fcn(time, t_inj,pulselength)
sine_wave = 0.003*sin(1000*2*pi*time);
droop = (1-(0.0125*time/(t_inj+pulselength)));
amp_fac = droop - sine_wave;
phase_diff = -12*pi/180*(1-amp_fac)/0.0125;
```

Figure A.5 The modulator Matlab code.

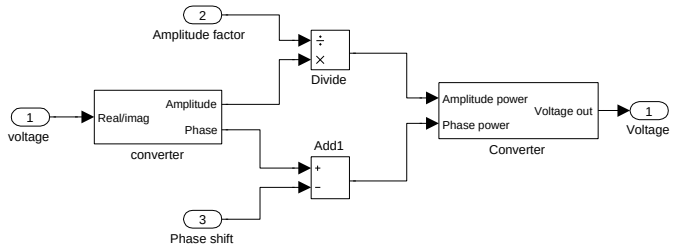

Figure A.6 The droop/ripple compensator block.

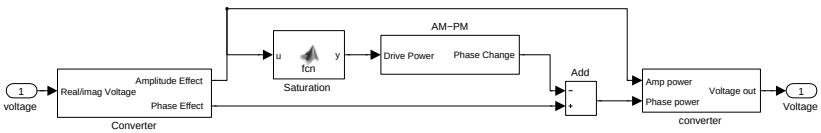

Figure A.7 The phase compensator block.

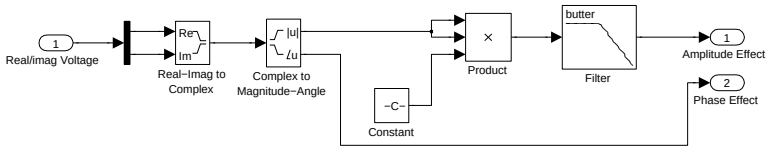

Figure A.8 The "Converter with filter" block inside the klystron model.

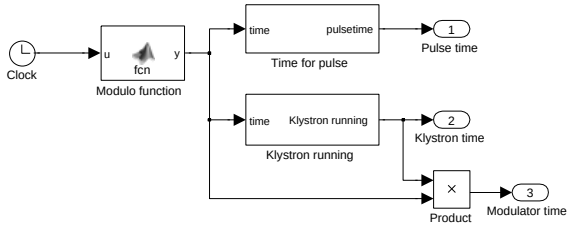

Figure A.9 The time generator block.

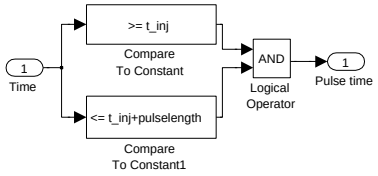

Figure A.10 The "Time for pulse" block inside the time generator block.

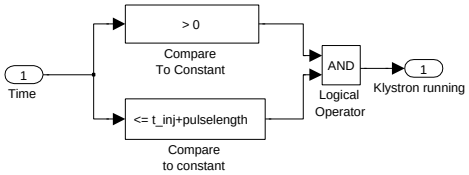

Figure A.11 The "Klystron running" block inside the time generator block.